A Lagrangian fluctuation–dissipation relation for scalar turbulence. Part II. Wall-bounded flows

Theodore D. Drivas[1,†] **and Gregory L. Eyink**[1,2]

[1]Department of Applied Mathematics and Statistics, The Johns Hopkins University,
Baltimore, MD 21218, USA

[2]Department of Physics and Astronomy, The Johns Hopkins University,
Baltimore, MD 21218, USA

We derive here Lagrangian fluctuation–dissipation relations for advected scalars in wall-bounded flows. The relations equate the dissipation rate for either passive or active scalars to the variance of scalar inputs from the initial values, boundary values and internal sources, as those are sampled backward in time by stochastic Lagrangian trajectories. New probabilistic concepts are required to represent scalar boundary conditions at the walls: the boundary local-time density at points on the wall where scalar fluxes are imposed and the boundary first hitting time at points where scalar values are imposed. These concepts are illustrated both by analytical results for the problem of pure heat conduction and by numerical results from a database of channel-flow turbulence, which also demonstrate the scalar mixing properties of near-wall turbulence. As an application of the fluctuation–dissipation relation, we examine for wall-bounded flows the relation between anomalous scalar dissipation and Lagrangian spontaneous stochasticity, i.e. the persistent non-determinism of Lagrangian particle trajectories in the limit of vanishing viscosity and diffusivity. In Part I of this series, we showed that spontaneous stochasticity is the only possible mechanism for anomalous dissipation of passive or active scalars, away from walls. Here it is shown that this remains true when there are no scalar fluxes through walls. Simple examples show, on the other hand, that a distinct mechanism of non-vanishing scalar dissipation can be thin scalar boundary layers near the walls. Nevertheless, we prove for general wall-bounded flows that spontaneous stochasticity is another possible mechanism of anomalous scalar dissipation.

Key words: mathematical foundations, turbulence theory, turbulent mixing

---

1. Introduction

This paper is the second in a series which initiates a new approach to the theory of turbulent scalar dissipation based upon a Lagrangian fluctuation–dissipation relation (FDR). This relation is derived within a representation of the scalar field by stochastic fluid particles, which naturally extends Lagrangian methods for ideally advected

† Email address for correspondence: tdrivas2@jhu.edu

scalars to realistic problems with both advection and diffusion. In Part I of the series (Drivas & Eyink 2017; hereafter, I) the stochastic representation and FDR were obtained for flows in finite domains without any boundaries. Using the FDR, we resolved an on-going controversy regarding the phenomenon of Lagrangian spontaneous stochasticity, or the persistent stochasticity of Lagrangian trajectories and breakdown of uniqueness of particle trajectories for high Reynolds numbers. In the ground-breaking work of Bernard, Gawędzki & Kupiainen (1998) on the Kraichnan (1968) model of turbulent advection, the property of Lagrangian spontaneous stochasticity was first discovered and shown to be a consequence of the classical (Richardson 1926) theory of turbulent particle dispersion. Bernard *et al.* (1998) furthermore showed that anomalous scalar dissipation within the Kraichnan model is due to spontaneous stochasticity. The validity of this concept for scalars advected by a true turbulent flow has, however, been strongly questioned (e.g. Tsinober 2009). A key result of Part I was the demonstration that spontaneous stochasticity is the only possible mechanism of anomalous dissipation for both passive and active scalars with any advecting velocity field whatsoever, away from walls.

Wall-bounded flows are, on the other hand, ubiquitous both in engineering applications and in nature. Nearly every turbulent flow encountered in our daily experience involves solid walls and obstacles that are either stationary or moving, flexible membranes or free surfaces. Geophysical turbulent flows are most commonly constrained by topography, basin boundaries or surfaces separating multiple phases (e.g. air–water). These boundaries can profoundly affect the organization of the turbulence and driving from the boundary is very often the origin of the turbulence itself. Thus, any perspective on turbulent scalar dissipation with a claim of generality must be applicable to flows with boundaries. Our aim in this work is to extend the approach and results of Part I to the most canonical examples of wall-bounded flows. To be specific, we consider a scalar field θ (such as temperature, dye concentration, etc.) transported by a fluid with velocity $\boldsymbol{u}$, governed by the advection–diffusion equation in the interior of a finite domain Ω:

$$\partial_t \theta + \boldsymbol{u} \cdot \boldsymbol{\nabla} \theta = \kappa \Delta \theta + S, \tag{1.1}$$

with appropriate conditions specified on the boundary $\partial \Omega$. Here $\kappa > 0$ is the molecular diffusivity of the scalar and $S(\boldsymbol{x}, t)$ is a bulk source field. Typical situations are those in which the scalar field is held fixed on the boundary (Dirichlet conditions), those in which the scalar flux through the wall is fixed (Neumann conditions) or a mixture of these along different parts of the boundary decomposed as $\partial \Omega = \partial \Omega_D \cup \partial \Omega_N$. More formally, for a function $\psi(\boldsymbol{x}, t)$ specifying scalar boundary values and a function $g(\boldsymbol{x}, t)$ specifying the fluxes through the wall, one solves (1.1) subject to the conditions

$$\text{Dirichlet:} \quad \theta(\boldsymbol{x}, t) = \psi(\boldsymbol{x}, t), \quad \boldsymbol{x} \in \partial \Omega_D \tag{1.2}$$

$$\text{Neumann:} \quad -\boldsymbol{\mu}(\boldsymbol{x}, t) \cdot \boldsymbol{\nabla} \theta(\boldsymbol{x}, t) = g(\boldsymbol{x}, t) \quad \boldsymbol{x} \in \partial \Omega_N, \tag{1.3}$$

where $\boldsymbol{\mu} = \kappa \boldsymbol{n}$ with $\boldsymbol{n}(\boldsymbol{x})$ being the unit inward normal to the boundary $\partial \Omega$. (All of our considerations in this paper apply with straightforward modifications to the more general situation where the scalar flux is given by an anisotropic Fick's law as $\boldsymbol{j}(\boldsymbol{x}, t) = -\boldsymbol{K}(\boldsymbol{x}, t) \boldsymbol{\nabla} \theta(\boldsymbol{x}, t)$ for a positive–definite, symmetric diffusivity tensor $\boldsymbol{K}$. In that case, the component of the flux normal to the boundary is $j_n = \boldsymbol{n} \cdot \boldsymbol{j} = -\boldsymbol{\mu} \cdot \boldsymbol{\nabla} \theta$ with the so-called 'co-normal vector' $\boldsymbol{\mu} = \boldsymbol{K} \boldsymbol{n}$ satisfying $\boldsymbol{\mu} \cdot \boldsymbol{n} = \boldsymbol{n}^\top \boldsymbol{K} \boldsymbol{n} > 0$.)

Additionally, appropriate boundary conditions must be specified for the velocity field at the wall. Throughout this paper, we consider the most common stick (or no-slip) boundary conditions:

$$\boldsymbol{u}(\boldsymbol{x}, t) = 0, \quad \boldsymbol{x} \in \partial\Omega. \tag{1.4}$$

We shall further discuss in this paper advection only by an incompressible fluid satisfying

$$\nabla \cdot \boldsymbol{u} = 0, \tag{1.5}$$

since only then does fluid advection conserve scalar integrals of the form $\int d^d x f(\theta(\boldsymbol{x}, t))$. However, we place no other general constraints on the velocity $\boldsymbol{u}$, which may obey, for example, an equation of motion involving θ itself. Thus, our considerations apply not only to passive but also to active scalar fields.

For all wall-bounded flows of the above classes we derive Lagrangian fluctuation–dissipation relations generalizing those in Part I and we exploit them to precisely characterize for wall-bounded flows the connection between Lagrangian spontaneous stochasticity and anomalous scalar dissipation. To avoid confusion, we note that our Lagrangian FDRs have no obvious relation to the fluctuation–dissipation theorems traditional in non-equilibrium statistical physics (see the discussion in Part I, §5). To our knowledge, both these FDRs and the results derived for wall-bounded flows have never been discussed previously, as all related works (e.g. Buaria, Yeung & Sawford 2016) discuss only flows without boundaries. These FDRs are obtained, however, within known stochastic representations for solutions of the scalar advection equation, with boundary conditions either of Dirichlet, Neumann or mixed form (see e.g. Soner 2007). Our discussion of the stochastic representations themselves involves only very modest originality and involves mainly a convenient compilation of existing results from multiple sources. The key concepts from probability theory to derive these representations are the boundary local-time density and the boundary hitting time, which are carefully described and illustrated with numerical results from a turbulent channel-flow simulation. The new FDRs derived within these representations express an exact balance between the time-averaged scalar dissipation and the input of stochastic scalar variance from the initial data, interior scalar sources and boundary conditions as these are sampled by stochastic Lagrangian trajectories backward in time.

With no-flux (zero Neumann) boundary conditions for the scalar, we obtain results identical to those of Bernard *et al.* (1998) for domains without a boundary: namely, spontaneous stochasticity is both necessary and sufficient for anomalous dissipation of a passive scalar, and necessary for anomalous dissipation of an active scalar. However, for general imposed fluxes (Neumann conditions), imposed scalar values at the wall (Dirichlet conditions) or mixed Dirichlet/Neumann conditions, the necessity statement is not generally true. Simple examples, such as pure thermal conduction with imposed heat fluxes at the walls, show that thin scalar boundary layers can in such flows provide an entirely distinct mechanism of non-vanishing scalar dissipation with a vanishing molecular diffusivity. Nevertheless, we obtain from our FDRs a lower bound on the passive scalar dissipation rate, which implies that spontaneous stochasticity is sufficient for anomalous dissipation. With some additional, physically plausible but unproven assumptions, we can extend this sufficiency statement also to active scalars. It thus remains true for all wall-bounded flows that spontaneous stochasticity is a viable source of anomalous scalar dissipation. This is the main theoretical result of the present paper. The potential of our FDRs is not, however,

exhausted by this single result and our paper sets up the framework for more general applications. In Part III of this series (Eyink & Drivas 2017) we apply our FDR to turbulent Rayleigh–Bénard convection and obtain a novel Lagrangian formulation of the Nusselt–Rayleigh scaling law.

The detailed contents of the present paper are as follows: in § 2, we derive the FDR in the case of wall-bounded flows with imposed scalar fluxes (§ 2.1) and we relate spontaneous stochasticity and anomalous dissipation (§ 2.3). The next section (§ 3) discusses flows with imposed scalar values at the wall and mixed conditions, deriving first an FDR inequality (§ 3.1), using it to relate spontaneous stochasticity to anomalous dissipation (§ 3.3), then deriving an FDR equality (§ 3.4) and lastly discussing mixed boundary conditions (§ 3.5). The numerical results for turbulent channel flow (§§ 2.2 and 3.2) serve not only to illustrate key probabilistic concepts for a fluid mechanics audience but also investigate the joint effects of turbulence and walls on scalar mixing rates, which are important in our subsequent study of Rayleigh–Bénard convection (III). In the summary and discussion § 4 we discuss some future challenges. Three appendices give further details, including analytical results for a test case of pure diffusion used to assess the effects of fluid advection (appendices A and B), rigorous details of the new proofs relating spontaneous stochasticity and anomalous dissipation (appendix C) and explanation of the numerical methods employed for our turbulent channel-flow studies (appendix D).

2. Imposed scalar fluxes at the wall

We consider in this section a scalar $\theta(\boldsymbol{x}, t)$ with pure Neumann boundary conditions ($\partial \Omega_N = \partial \Omega$), satisfying

$$\left. \begin{array}{ll} \partial_t \theta + \boldsymbol{u} \cdot \nabla \theta = \kappa \Delta \theta + S & \boldsymbol{x} \in \Omega, \\ -\boldsymbol{\mu}(\boldsymbol{x}, t) \cdot \nabla \theta(\boldsymbol{x}, t) = g(\boldsymbol{x}, t) & \boldsymbol{x} \in \partial \Omega \end{array} \right\} \tag{2.1}$$

for given initial data θ_0, source field S, flux function g and co-normal vector field $\boldsymbol{\mu}$.

2.1. *Stochastic representation and fluctuation–dissipation relation*

The stochastic representation of solutions of pure Neumann problems has been discussed in many earlier publications, such as Freĭdlin (1985), Burdzy, Chen & Sylvester (2004) and Soner (2007) on fundamental mathematical theory and Mil'shtein (1996), Keanini (2007) and Słomiński (2013) for numerical methods. In order to impose Neumann conditions, essentially, one averages over stochastic trajectories which reflect off the boundary of the domain, contributing to the solution a correction related to their sojourn time on the walls. We briefly review the subject here. Our presentation is somewhat different than in any of the above references and, in particular, is based on backward stochastic integration theory. This framework yields, in our view, the simplest and most intuitive derivations. We also specify appropriate physical dimensions for all quantities, whereas the mathematical literature is generally negligent about physical dimensions and studies only the special value of the diffusivity $\kappa = 1/2$, in unspecified units. We have been careful to restore a general value of the diffusivity κ in all positions where it appears.

The fundamental notion of the representation is the boundary local time density $\tilde{\ell}_{t,s}(\boldsymbol{x})$ (Stroock & Varadhan 1971; Lions & Sznitman 1984; Burdzy *et al.* 2004), which, for a stochastic Lagrangian particle located at $\boldsymbol{x} \in \Omega$ at time t, is the time

within the interval $[s, t]$ which is spent near the boundary $\partial\Omega$ per unit distance. Its physical units are thus (time)/(length) or 1/(velocity). Note that we consider here the backward-in-time process, whereas Burdzy *et al.* (2004) employed the forward-time process and time reflection to derive an analogous representation. We thus take the boundary local-time density to be a non-positive non-increasing random process which decreases (backward in time) only when the stochastic particle is on the boundary. This stochastic process is defined via the 'Skorohod problem', in conjunction with the (backward) stochastic flow $\tilde{\boldsymbol{\xi}}_{t,s}^{\nu,\kappa}(\boldsymbol{x})$ with reflecting boundary conditions which satisfies

$$\hat{\mathrm{d}}\tilde{\boldsymbol{\xi}}_{t,s}(\boldsymbol{x}) = \boldsymbol{u}^{\nu}(\tilde{\boldsymbol{\xi}}_{t,s}(\boldsymbol{x}), s)\,\mathrm{d}s + \sqrt{2\kappa}\,\hat{\mathrm{d}}\widetilde{\boldsymbol{W}}_s - \boldsymbol{\mu}(\tilde{\boldsymbol{\xi}}_{t,s}(\boldsymbol{x}), s)\,\hat{\mathrm{d}}\tilde{\ell}_{t,s}(\boldsymbol{x}), \tag{2.2}$$

with $\tilde{\boldsymbol{\xi}}_{t,t}(\boldsymbol{x}) = \boldsymbol{x}$ as usual. The boundary local time is then given by the formula

$$\tilde{\ell}_{t,s}(\boldsymbol{x}) = \int_t^s \mathrm{d}r\delta(\mathrm{dist}(\tilde{\boldsymbol{\xi}}_{t,r}(\boldsymbol{x}), \partial\Omega)) \equiv \lim_{\varepsilon\to 0}\frac{1}{\varepsilon}\int_t^s \mathrm{d}r\chi_{\partial\Omega_\varepsilon}(\tilde{\boldsymbol{\xi}}_{t,r}(\boldsymbol{x})), \quad s < t, \tag{2.3}$$

in terms of an 'ε-thickened boundary'

$$\partial\Omega_\varepsilon = \{\boldsymbol{x}\in\Omega : \mathrm{dist}(\boldsymbol{x}, \partial\Omega) < \varepsilon\}. \tag{2.4}$$

See Burdzy *et al.* (2004, Theorem 2.6). (Note that (2.7) of Burdzy *et al.* (2004) contains an additional factor of 1/2, because their local-time density is our $\kappa\tilde{\ell}_{t,s}(\boldsymbol{x})$ and they consider only the case $\kappa = 1/2$.) In (2.3) we denote by χ_A the characteristic function of a set defined as

$$\chi_A(\boldsymbol{x}) = \begin{cases} 1 & x \in A \\ 0 & x \notin A. \end{cases} \tag{2.5}$$

Lions & Sznitman (1984) have proved existence and uniqueness of stochastic processes as strong solutions to this 'Skorohod problem' with Lipschitz velocity fields $\boldsymbol{u}$ and sufficient regular normal vectors $\boldsymbol{n}$ at a smooth boundary. Of some interest for the consideration of non-smooth velocity fields that might appear in the limit $\nu \to 0$, Stroock & Varadhan (1971) obtain stochastic process solutions when $\boldsymbol{u}$ is merely bounded, measurable and establish uniqueness in law, i.e. uniqueness of probability distributions. The spatial regularity in $\boldsymbol{x}$ of the processes $(\tilde{\boldsymbol{\xi}}_{t,s}(\boldsymbol{x}), \tilde{\ell}_{t,s}(\boldsymbol{x}))$ defined jointly as above is the subject of recent works on stochastic flows with reflecting boundary conditions (Pilipenko 2005, 2014; Burdzy 2009). Note that the stochastic particles described by $\tilde{\boldsymbol{\xi}}_{t,s}(\boldsymbol{x})$ are reflected in the direction of $\boldsymbol{\mu}$ when they hit the wall, thus staying forever within Ω, and the flow preserves the volume within the domain when $\nabla\cdot\boldsymbol{u}^\nu = 0$, as assumed here. It follows formally from (2.3) that the boundary local-time density can be written as

$$\tilde{\ell}_{t,s}(\boldsymbol{x}) = \int_t^s \mathrm{d}r\int_{\partial\Omega}\mathrm{d}H^{d-1}(\boldsymbol{z})\delta^d(\boldsymbol{z} - \tilde{\boldsymbol{\xi}}_{t,r}(\boldsymbol{x})), \tag{2.6}$$

where H^{d-1} is the $(d-1)$-dimensional Hausdorff measure (surface area) over the smooth boundary $\partial\Omega$ of the domain. We have not found this intuitive formula anywhere in the probability theory literature, but it should be possible to prove rigorously with suitable smoothness assumptions on the boundary.

By means of the above notions one can obtain a stochastic representation for solutions to the initial-value problem of the system (2.1). The backward Itō formula (Kunita 1997; Friedman 2006) applied to $\theta(\tilde{\boldsymbol{\xi}}_{t,s}(\boldsymbol{x}), s)$ gives

$$\hat{\mathrm{d}}\theta(\tilde{\boldsymbol{\xi}}_{t,s}(\boldsymbol{x}), s) = [(\partial_s\theta + \boldsymbol{u}\cdot\nabla\theta - \kappa\Delta\theta)\mathrm{d}s - (\nabla\theta\cdot\boldsymbol{\mu})\hat{\mathrm{d}}\tilde{\ell}_{t,s} + \sqrt{2\kappa}\,\hat{\mathrm{d}}\widetilde{\boldsymbol{W}}_s\cdot\nabla\theta]_{(\tilde{\boldsymbol{\xi}}_{t,s}(\boldsymbol{x}),s)}$$

$$= S(\tilde{\boldsymbol{\xi}}_{t,s}(\boldsymbol{x}), s)\mathrm{d}s + g(\tilde{\boldsymbol{\xi}}_{t,s}(\boldsymbol{x}), s)\hat{\mathrm{d}}\tilde{\ell}_{t,s} + \sqrt{2\kappa}\,\hat{\mathrm{d}}\widetilde{\boldsymbol{W}}_s\cdot\nabla\theta(\tilde{\boldsymbol{\xi}}_{t,s}(\boldsymbol{x}), s), \quad (2.7)$$

where in the second line we have used the fact that $\theta(\boldsymbol{x}, s)$ solves the boundary-value problem (2.1). We find upon integration from 0 to t,

$$\theta(\boldsymbol{x}, t) = \theta_0(\tilde{\boldsymbol{\xi}}_{t,0}(\boldsymbol{x})) + \int_0^t \mathrm{d}s\, S(\tilde{\boldsymbol{\xi}}_{t,s}(\boldsymbol{x}), s) + \int_0^t g(\tilde{\boldsymbol{\xi}}_{t,s}(\boldsymbol{x}), s)\,\hat{\mathrm{d}}\tilde{\ell}_{t,s}$$

$$+ \sqrt{2\kappa}\int_0^t \hat{\mathrm{d}}\widetilde{\boldsymbol{W}}_s\cdot\nabla\theta(\tilde{\boldsymbol{\xi}}_{t,s}(\boldsymbol{x}), s) \quad (2.8)$$

and thus expectation over the Brownian motion yields the representation

$$\theta(\boldsymbol{x}, t) = \mathbb{E}\left[\theta_0(\tilde{\boldsymbol{\xi}}_{t,0}(\boldsymbol{x})) + \int_0^t \mathrm{d}s\, S(\tilde{\boldsymbol{\xi}}_{t,s}(\boldsymbol{x}), s) + \int_0^t g(\tilde{\boldsymbol{\xi}}_{t,s}(\boldsymbol{x}), s)\,\hat{\mathrm{d}}\tilde{\ell}_{t,s}\right]. \quad (2.9)$$

By means of (2.6), this formula can be written equivalently in terms of the transition probability density function $p^{v,\kappa}(\boldsymbol{y}, s|\boldsymbol{x}, t) = \mathbb{E}[\delta^d(\tilde{\boldsymbol{\xi}}_{t,s}^{v,\kappa}(\boldsymbol{x}) - \boldsymbol{y})]$ for the reflected particle to be at position $\boldsymbol{y}$ at time $s < t$, given that it was at position $\boldsymbol{x}$ at time t:

$$\theta(\boldsymbol{x}, t) = \int_\Omega \mathrm{d}^d\boldsymbol{x}_0\, \theta_0(\boldsymbol{x}_0)p(\boldsymbol{x}_0, 0|\boldsymbol{x}, t) + \int_0^t \mathrm{d}s\int_\Omega \mathrm{d}^d\boldsymbol{y}\, S(\boldsymbol{y}, s)\, p(\boldsymbol{y}, s|\boldsymbol{x}, t)$$

$$+ \int_0^t \mathrm{d}s\int_{\partial\Omega} \mathrm{d}H^{d-1}(\boldsymbol{z})\, g(\boldsymbol{z}, s)\, p(\boldsymbol{z}, s|\boldsymbol{x}, t). \quad (2.10)$$

Clearly, the scalar value $\theta(\boldsymbol{x}, t)$ is an average of the randomly sampled initial data and the scalar inputs from the internal source and the scalar flux through the boundary along a random history backward in time.

Just as for domains without walls in Part I, we introduce a stochastic scalar field which represents the contribution for a specific stochastic Lagrangian trajectory

$$\tilde{\theta}(\boldsymbol{x}, t) \equiv \theta_0(\tilde{\boldsymbol{\xi}}_{t,0}(\boldsymbol{x})) + \int_0^t \mathrm{d}s\, S(\tilde{\boldsymbol{\xi}}_{t,s}(\boldsymbol{x}), s) + \int_0^t g(\tilde{\boldsymbol{\xi}}_{t,s}(\boldsymbol{x}), s)\,\hat{\mathrm{d}}\tilde{\ell}_{t,s}, \quad (2.11)$$

that now includes the boundary-flux term, so that $\theta(\boldsymbol{x}, t) = \mathbb{E}[\tilde{\theta}(\boldsymbol{x}, t)]$ (For all $s < t$ the quantity $\tilde{\theta}(\boldsymbol{x}, t; s) = \theta(\tilde{\boldsymbol{\xi}}_{t,s}(\boldsymbol{x}), s) + \int_s^t S(\tilde{\boldsymbol{\xi}}_{t,r}(\boldsymbol{x}), r)\,\mathrm{d}r + \int_s^t g(\tilde{\boldsymbol{\xi}}_{t,r}(\boldsymbol{x}), r)\,\hat{\mathrm{d}}\tilde{\ell}_{t,r}$ is equal to $\theta(\boldsymbol{x}, t) - \sqrt{2\kappa}\int_s^t \hat{\mathrm{d}}\widetilde{\boldsymbol{W}}_r\cdot\nabla\theta(\tilde{\boldsymbol{\xi}}_{t,r}(\boldsymbol{x}), r)$, analogous to (2.8). It is thus a martingale backward in time, i.e. it is statistically conserved and, on average, equals $\theta(\boldsymbol{x}, t)$ for all $s < t$. Clearly, $\tilde{\theta}(\boldsymbol{x}, t) = \tilde{\theta}(\boldsymbol{x}, t; 0)$. This backward martingale property shows that the stochastic representation employed here is a natural generalization to diffusive advection of the standard deterministic Lagrangian representation for non-diffusive, smooth advection). As in Part I, we warn the reader that the quantity $\tilde{\theta}(\boldsymbol{x}, t)$ is entirely different from the conventional 'turbulent' scalar fluctuation $\theta'(\boldsymbol{x}, t)$ defined with respect to ensembles of scalar initial conditions, advecting velocities

or random sources. An application of the Itō-isometry (see Oksendal 2013, § 3.1) exactly as in Part I yields for the scalar variance

$$\frac{1}{2}\text{Var}[\tilde{\theta}(\boldsymbol{x}, t)] = \kappa \ \mathbb{E} \int_0^t \mathrm{d}s \ |\boldsymbol{\nabla}\theta(\tilde{\boldsymbol{\xi}}_{t,s}(\boldsymbol{x}), s)|^2, \tag{2.12}$$

which is a local version of our FDR. Integrating over the bounded domain and invoking volume preservation by the reflected flow, we obtain

$$\frac{1}{2}\langle\text{Var} \ \tilde{\theta}(t)\rangle_\Omega = \kappa \int_0^t \mathrm{d}s \ \langle|\boldsymbol{\nabla}\theta(s)|^2\rangle_\Omega . \tag{2.13}$$

This, together with (2.11), is our exact FDR for scalars (either passive or active) with general Neumann boundary conditions. Just as for (2.20) of Part I in the case of domains without walls, we obtain for the infinite-time limit of the local scalar variance

$$\lim_{t\to\infty} \frac{1}{2t}\text{Var}[\tilde{\theta}(\boldsymbol{x}, t)] = \langle\kappa|\boldsymbol{\nabla}\theta|^2\rangle_{\Omega,\infty}, \quad \text{for all } \boldsymbol{x} \in \Omega, \tag{2.14}$$

when the reflected stochastic particle wanders ergodically over the flow domain Ω. This will generally be true when $\kappa > 0$, and the ergodic average thus coincides with the average over the stationary distribution of the particle. This is uniform (Lebesgue) measure because of incompressibility of the flow. The long-time limit is thus independent of the space point $\boldsymbol{x}$. We shall not make use of (2.14) in the present work, but it plays a central role in our analysis of steady-state turbulent convection in Part III.

2.2. *Numerical results*

To provide some additional insight into these concepts, we present in appendix A an elementary analytical example: pure diffusion on a finite interval with a constant scalar flux imposed at the two ends. To be concrete, we shall use the language of heat conduction, and thus refer to temperature field, heat flux, etc. In addition, we present now some numerical results on stochastic Lagrangian trajectories and boundary local-time densities for a proto-typical wall-bounded flow, turbulent channel flow. These numerical results are directly relevant to turbulent thermal transport in a channel with imposed heat fluxes at the walls. They also have relevance to the problem of Rayleigh–Bénard convection which will be discussed in Part III, since channel flow provides the simplest example of a turbulent shear flow with a logarithmic law of the wall of the type conjectured to exist at very high Rayleigh numbers in turbulent convection (Kraichnan 1962). For the purpose of our study, we use the $Re_\tau = 1000$ channel-flow dataset in the Johns Hopkins Turbulence Database (see Graham *et al.* (2016) and http://turbulence.pha.jhu.edu). We follow the notation in these references and, in particular, the x direction is streamwise, y is wall-normal and z is spanwise. For the details of our numerical methods, see appendix D.1. We plot in figure 1 for three choices of Prandtl number ($Pr = 0.1$, 1, 10) a single realization of $(\tilde{\boldsymbol{\xi}}_{t,s}(\boldsymbol{x}), \tilde{\ell}_{t,s}(\boldsymbol{x}))$ for a stochastic particle released at a point $\boldsymbol{x}$ on the lower wall $y = -h$ at the final time t_f in the database, then evolved backward in time. Using Cartesian coordinates $\tilde{\boldsymbol{\xi}}_{t,s} = (\tilde{\xi}_{t,s}, \tilde{\eta}_{t,s}, \tilde{\zeta}_{t,s})$, figure 1(*a*) plots the wall-normal particle position $\tilde{\eta}_{t,s}(\boldsymbol{x})$ as height above the wall $\Delta y = y + h$ and the right panel plots the local-time density $\tilde{\ell}_{t,s}(\boldsymbol{x})$, both as functions of shifted time $s - t_f$. All quantities are expressed in wall units, in terms
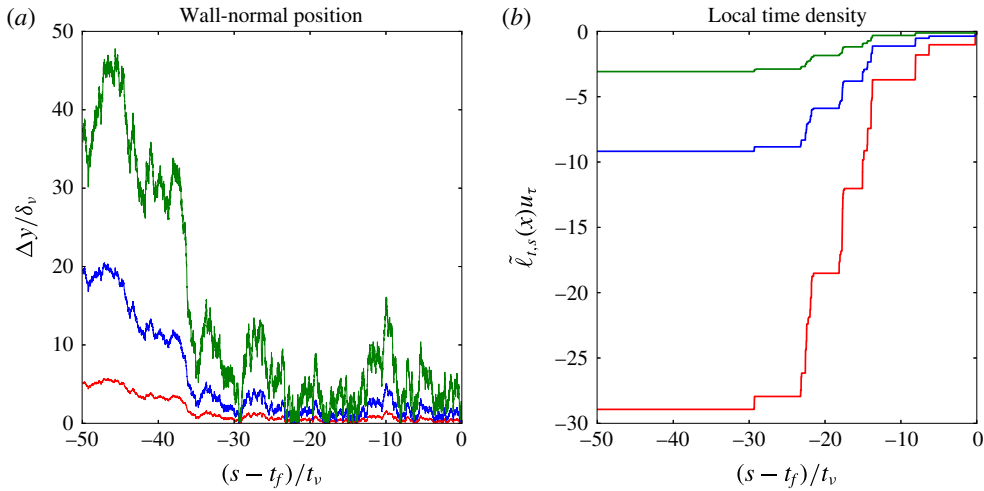
FIGURE 1. (Colour online) Realizations of wall-normal position (*a*) and local-time density process (*b*) for a particle released on the lower wall at $(x, z) = (3543.84\delta_\nu, 1891.56\delta_\nu)$ for Prandtl values $Pr = 0.1$ (green, medium), 1.0 (blue, heavy) and 10 (red, light).

of the friction velocity u_τ, the viscous length $\delta_\tau = \nu/u_\tau$ and the viscous time $\tau_\nu = \nu/u_\tau^2$. Important features to observe in figure 1 are the jumps in the local-time density at the instants when the particles are incident upon the wall and reflected. These incidences occur predominantly near the release time and eventually cease (backward in time) as the particles are transported away from the wall. This escape from the wall occurs slower for smaller κ or larger Pr, and the local times at the wall are correspondingly larger magnitude for larger Pr.

We next discuss statistics of the entire ensemble of stochastic particles for two specific release points at the wall, one point selected inside a low-speed streak and the other a high-speed streak. We are especially interested here in the role of turbulence in enhancing heat transport away from the wall, compared with pure thermal diffusion. It has sometimes between questioned whether turbulence close to the wall indeed increases thermal transport, because of the restrictions imposed on the vertical motions (e.g. Niemela & Sreenivasan 2003, §7.2). We thus select two points, one in a low-speed streak with mean motion toward the wall (backward in time) and the other in a high-speed streak with mean motion away from the wall (backward in time). Comparing these two points helps to identify any possible strictures on turbulent transport imposed by the solid wall. The selection is illustrated in figure 2, which plots the streamwise velocity in the buffer layer at distance $\Delta y = 10\delta_\tau$ above the bottom channel wall. The low-speed streaks associated with 'ejections' from the wall and high-speed streaks associated with 'sweeps' toward the wall seen there are characteristic of turbulent boundary layers (Kline *et al.* 1967). The *x–z* coordinates of the two release points are indicated by the diamonds ($\Diamond$) in figure 2 (and note that the point selected in the low-speed streak is that featured in the previous figure 1). For each of these two release points and for the three choices of Prandtl number $Pr = 0.1, 1, 10$, we used $N = 1024$ independent solutions of equations (2.2) and (2.3) to calculate the dispersion of the stochastic trajectories and the probability density functions (PDFs) of the local-time densities backward in time. Error bars in the plots represent the standard error of the mean (s.e.m.) for the *N*-sample averages and in addition, for the PDFs, the effects of variation in kernel density bandwidth.
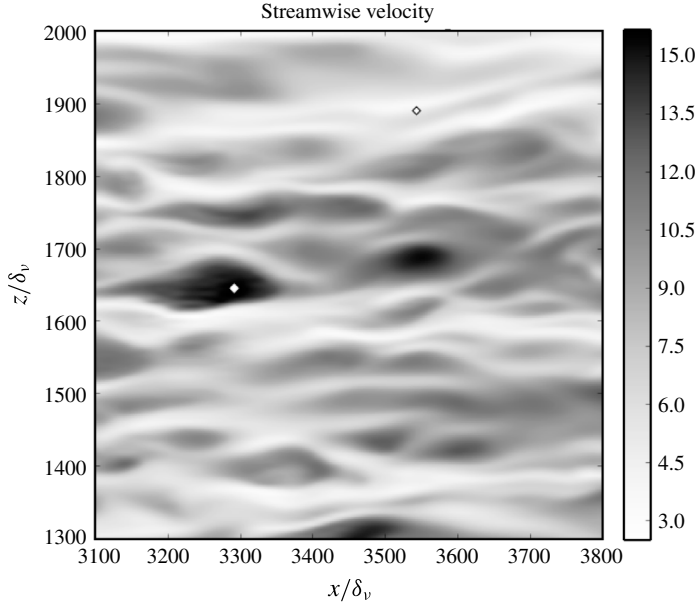
FIGURE 2. Streamwise velocity at normal distance $\Delta y = 10\delta_v$ from the lower wall non-dimensionalized by the friction velocity u_τ. The open diamonds ($\Diamond$) mark the (x, z) coordinates, $(3291.73\delta_v, 1644.98\delta_v)$ and $(3543.84\delta_v, 1891.56\delta_v)$, of the selected release points at wall-parallel positions of high-speed (dark) and low-speed (light) streaks, respectively.

In figure 3(*a*,*b*), we show 30 representative particle trajectories for the two release points (left within a high-speed streak, right in a low-speed) and for each of the three Prandtl numbers. By eye, the ensembles of trajectories for the three different Prandtl numbers appear quite similar. In figure 3(*c*,*d*), we plot the mean-squared dispersion of the stochastic particles for the two release points and the three Prandtl numbers. There is an initial period (backward in time) where the dispersion grows with $\hat{s} = t_f - s$ as $4\kappa(3 - 2/\pi)\hat{s}$, which is the analytical result for a three-dimensional Brownian motion reflected from a plane (if $\tilde{W}(t)$ is standard one-dimensional Brownian motion with diffusivity κ, then $|\tilde{W}(t)|$ is the Brownian motion reflected at 0 and it is elementary to show that $\mathbb{E}^{1,2}[\{|\tilde{W}^{(1)}(t)| - |\tilde{W}^{(2)}(t)|\}^2] = 4\kappa(1 - 2/\pi)t$). There is then a cross-over to a limited regime of super-ballistic separation that is close to $\hat{s}^3$-growth. At still larger $\hat{s}$, the growth clearly slows but remains super-ballistic. Recall from Part I that Richardson dispersion with a cubic growth of dispersion is the physical mechanism of spontaneous stochasticity in homogeneous, isotropic turbulence. It would be quite surprising to observe Richardson dispersion in this channel-flow dataset, since the energy spectra published in Graham *et al.* (2016) and http://turbulence.pha.jhu.edu show that the Reynolds number is still too low to support a Kolmogorov-type inertial range. We believe that the cubic power-law growth observed arises instead from a simple combination of stochastic diffusion and mean shear, a molecular version of the turbulent shear dispersion discussed by Corrsin (1953). A toy model which illustrates this mechanism is a two-dimensional shear flow with $\boldsymbol{u}(\boldsymbol{x}) = (Sy, 0)$, where

$$\mathrm{d}\tilde{\xi}_t = S\tilde{\eta}_t + \sqrt{2\kappa}\ \mathrm{d}\tilde{W}_x(t), \quad \mathrm{d}\tilde{\eta}_t = \sqrt{2\kappa}\ \mathrm{d}\tilde{W}_y(t). \qquad (2.15a,b)$$
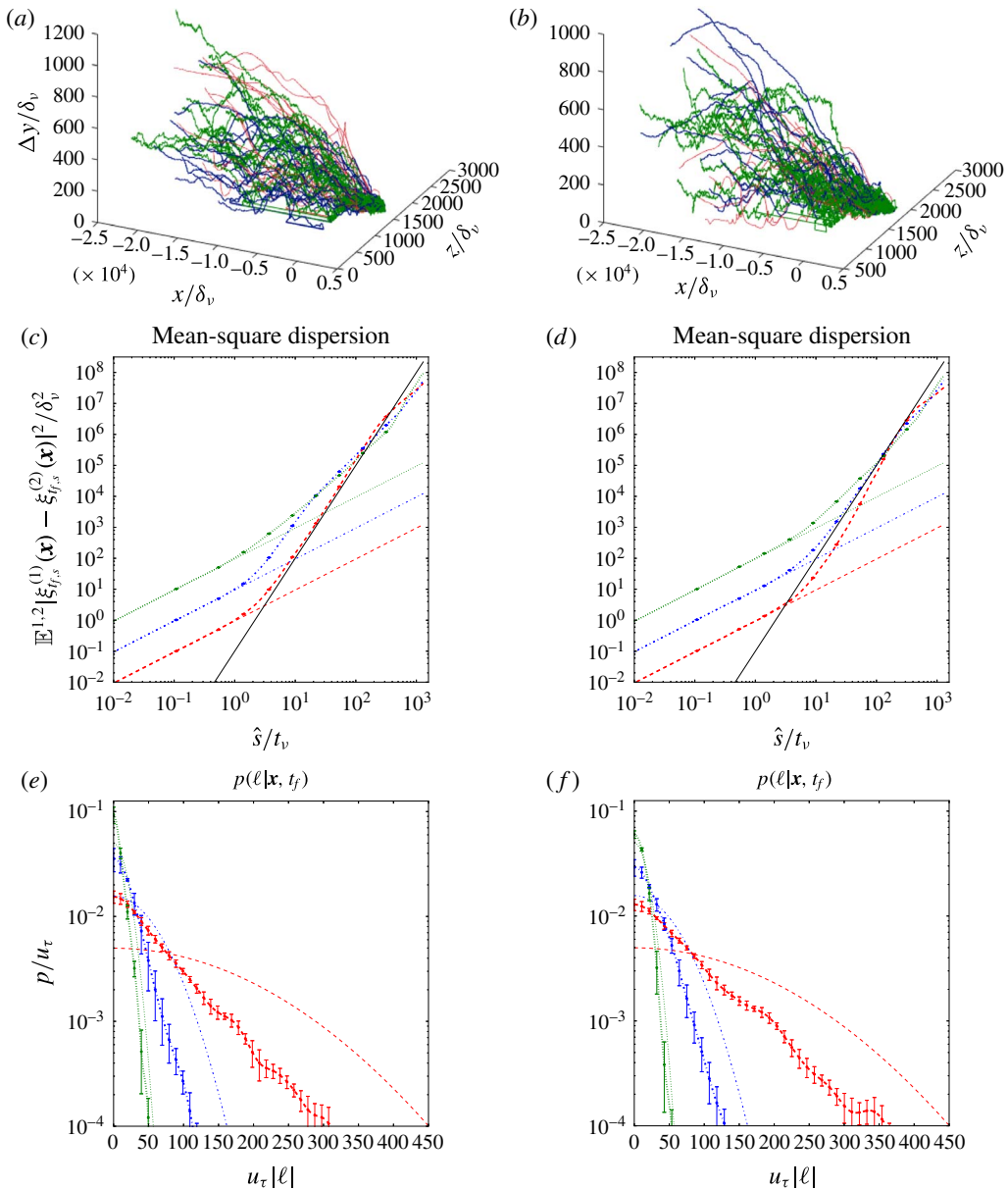
FIGURE 3. (Colour online) (*a,c,e*) Are for release at bottom wall near a high-speed streak, (*b,d,f*) for release near a low-speed streak. See markers on figure 2. (*a,b*) Show 30 representative reflected stochastic trajectories for $Pr = 0.1$ (green, medium), 1.0 (blue, heavy) and 10 (red, light). (*c,d*) Plot particle dispersion (heavy) and short-time results $4\kappa(3 - 2/\pi)\hat{s}$ (light) for each Pr with $Pr = 0.1$ (green, dot, $\cdots\cdots$), 1.0 (blue, dash-dot, $— \cdot —$) and 10 (red, dash, - - - -) and a plot (black,solid, ——) of $g(\nu/\tau_\nu^2)\hat{s}^3$ with $g = 0.1$. (*e,f*) Plot PDFs of (absolute values of) boundary local times for channel flow (heavy) and pure diffusion (light) for the three Pr values with the same line styles as (*c,d*).

Integration gives $\tilde{\xi}_t = \sqrt{2\kappa}\,(S\int_0^t \tilde{W}_y(s)\,\mathrm{d}s + \tilde{W}_x(t))$ and $\tilde{\eta}_t = \sqrt{2\kappa}\,\tilde{W}_y(t)$ when $(\tilde{\xi}_0, \tilde{\eta}_0) = (0,0)$, and the shear contributes a t^3-term to the x-component of the dispersion:

$$\mathbb{E}^{1,2}|\tilde{\xi}_t^{(1)} - \tilde{\xi}_t^{(2)}|^2 = 4\kappa\left(t + \tfrac{1}{3}S^2 t^3\right). \tag{2.16}$$

See Schütz & Bodenschatz (2016) for a very similar discussion of cubic-in-time dispersion in the context of bounded shear flows and weakly turbulent Rayleigh-Bénard convection in two dimensions. In the toy model (2.15*a,b*) the *y*-component of dispersion grows only diffusively. In qualitative agreement with this simple model, we have found that the cubic power-law growth in the channel-flow particle dispersion indeed arises solely from the streamwise component of the particle separation vector. We do not show this here, but the effect can be observed in the particle trajectories plotted in figure 3(*a,b*), where the particles are dispersed farthest along the streamwise direction. The t^3 dispersion in (2.16) differs notably from Richardson dispersion in that it is proportional to κ and it produces no spontaneous stochasticity, since it vanishes as $\kappa \to 0$. In the channel-flow $\hat{s}^3$-regime in figure 3(*c,d*) ($10^1 \lesssim \hat{s}/t_\eta \lesssim 10^2$) there is likewise an observable dependence on the diffusivity. These cautionary results are an admonition against interpreting any cubic or super-ballistic growth of pair separation whatsoever as evidence of spontaneous stochasticity. Richardson dispersion produces spontaneous stochasticity because of non-smooth relative advection, not simply because of super-ballistic separation.

In figure 3(*e,f*), we plot PDFs of the local-time density $\tilde{\ell}_{t_f,0}(\boldsymbol{x})$ accumulated backward over the entire time interval of the channel-flow database (one flow-through time), for the two release points and the three values of Prandtl number. As could be expected, smaller κ (or larger *Pr*) correspond to more time at the wall and a PDF supported on larger local-time densities. Comparing the results for the two release points, it can be seen that particles starting on the wall inside the high-speed streak tend to spend somewhat less time near the wall than those starting near the low-speed streak. This is easy to understand, if one recalls that low-speed streaks correspond to 'ejections' from the wall and high-speed streaks to 'sweeps' toward the wall. Backward in time, however, the fluid motions are exactly reversed. Thus, particles starting at the wall inside high-speed streaks are being swept away from the wall by the fluid motion backward in time, and those starting inside low-speed streaks are brought toward the wall. However, the location of the release point has a quite small effect on the PDF of the local-time density accumulated over one flow-through time, and it is plausible that this effect would be reduced by taking t_f even larger.

Finally, we have also plotted in figure 3(*e,f*) the analytical results for the local-time PDFs of a pure Brownian motion with diffusivity κ that is reflected from a planar wall (see appendix A.3 and (2.25) below). Compared with these results for Brownian motion, the corresponding channel-flow local-time PDFs exhibit in all cases a substantial reduction of time spent at the wall. These results show that turbulent fluctuations enhance transport away from the wall, even when the local flow initially carries the particles toward the wall (backward in time). Although we show these results only for two release points here, we have observed similar behaviour at all other locations on the wall that we have examined. This observation has importance for the problem of turbulent convection, where it was it was argued by Kraichnan (1962) that '... the effect of the small-scale turbulence that arises locally in the shear boundary layer should be to increase heat transport'. We shall return to this issue in Part III.

2.3. *Spontaneous stochasticity and anomalous dissipation*

As an application of our FDR (2.13) for flows with imposed scalar fluxes at the walls, we now discuss the equivalence between spontaneous stochasticity and anomalous scalar dissipation in this context. As we shall see, the effects of the walls can be profound.

The simplest situation is the case of vanishing wall fluxes, $g \equiv 0$, which corresponds to insulating/adiabatic walls when the scalar is the temperature and to impermeable walls when the scalar is the concentration of an advected substance (e.g. a dye, aerosol, etc.). In this case, the flux contribution proportional to the local-time density in (2.11) vanishes, and our FDR then becomes simply

$$\frac{1}{2} \left\langle \text{Var} \left[\theta_0(\tilde{\boldsymbol{\xi}}_{t,0}) + \int_0^t \mathrm{d}s \; S(\tilde{\boldsymbol{\xi}}_{t,s}, s) \right] \right\rangle_\Omega = \kappa \int_0^t \mathrm{d}s \left\langle |\nabla \theta(s)|^2 \right\rangle_\Omega. \quad (2.17)$$

This is formally identical to the relation (2.9) and (2.12) of Part I for flows in domains without boundaries, with the simple stochastic flow replaced by a reflected stochastic flow. We can therefore repeat verbatim the arguments from Part I, § 4 to conclude that, for walls that do not support fluxes, spontaneous stochasticity is equivalent to anomalous dissipation for passive scalars and for active scalars spontaneous stochasticity is (at least) necessary for anomalous scalar dissipation. For the sake of completeness, we briefly review the main ideas of this argument here. Assuming that $S \equiv 0$ for simplicity, the left-hand side of the FDR (2.17) becomes

$$\begin{aligned}
\text{Var}[\theta_0(\tilde{\boldsymbol{\xi}}_{t,0}(\boldsymbol{x}))] = \int \mathrm{d}^d x_0 \int \mathrm{d}^d x_0' \; \theta_0(\boldsymbol{x}_0)\theta_0(\boldsymbol{x}_0') \\
\times \left[p_2^{\nu,\kappa}(\boldsymbol{x}_0, 0; \boldsymbol{x}_0', 0|\boldsymbol{x}, t) - p^{\nu,\kappa}(\boldsymbol{x}_0, 0|\boldsymbol{x}, t)p^{\nu,\kappa}(\boldsymbol{x}_0', 0|\boldsymbol{x}, t) \right], \quad (2.18)
\end{aligned}$$

where we have introduced the 2-time (backward-in-time) transition density

$$p_2^{\nu,\kappa}(\boldsymbol{y}, s; \boldsymbol{y}', s'|\boldsymbol{x}, t) = \mathbb{E}[\delta^d(\boldsymbol{y} - \tilde{\boldsymbol{\xi}}_{t,s}^{\nu,\kappa}(\boldsymbol{x}))\delta^d(\boldsymbol{y}' - \tilde{\boldsymbol{\xi}}_{t,s'}^{\nu,\kappa}(\boldsymbol{x}))], \quad s, s' < t. \quad (2.19)$$

It can be shown using Young measure techniques that, at least along suitably chosen subsequences, the transition probabilities approach limiting values $p^*(\boldsymbol{y}, s; \boldsymbol{y}', s|\boldsymbol{x}, t)$, $p^*(\boldsymbol{y}, s|\boldsymbol{x}, t)$ as $\nu, \kappa \to 0$ whenever the flow domain is compact (Part I, appendix A.1). If in this limit the Lagrangian particle positions $\boldsymbol{\xi}_{t,s}^*$ are deterministic, then the 2-time transition probability factorizes:

$$p_2^*(\boldsymbol{y}, s; \boldsymbol{y}', s'|\boldsymbol{x}, t) = \delta^d(\boldsymbol{y} - \boldsymbol{\xi}_{t,s}^*(\boldsymbol{x}))\delta^d(\boldsymbol{y}' - \boldsymbol{\xi}_{t,s'}^*(\boldsymbol{x})) = p^*(\boldsymbol{y}, s|\boldsymbol{x}, t)p^*(\boldsymbol{y}', s'|\boldsymbol{x}, t). \quad (2.20)$$

Thus, non-factorization in the limit $\nu, \kappa \to 0$ is the signature of spontaneous stochasticity, i.e. of the limiting particle positions $\boldsymbol{\xi}_{t,s}^*$ remaining random as $\nu, \kappa \to 0$. Note that the variance (2.17) can only be non-vanishing in the limit if factorization fails. Consequently, anomalous dissipation requires spontaneous stochasticity. This is true both for passive and for active scalars. In the other direction, if there is spontaneous stochasticity on a positive-measure set of $\boldsymbol{x} \in \Omega$, one can choose (at least for passive scalars) a suitable θ_0 which will make the variance (2.17) positive. This implies a positive lower bound to the cumulative, volume-integrated scalar dissipation through the FDR (2.17). Thus spontaneous stochasticity and anomalous scalar dissipation are seen to be equivalent. See Part I, appendix A.2 for detailed mathematical proofs of these claims.

This result is relevant for many physical situations, such as a dye injected into a turbulent Taylor–Couette flow. The commonplace example of cream stirred into coffee is also essentially of this type, since the cup walls and surface of the stirrer are impermeable boundaries and there is also no transport of cream across the free fluid surface. The extension of our FDR (2.17) to problems with moving walls and free fluid surfaces should be relatively straightforward (and, indeed, the main result of the paper of Burdzy *et al.* (2004) was the construction of reflected Brownian processes for domains enclosed by moving boundaries). In all of these situations, any evidence for anomalous scalar dissipation is also evidence for (requires) spontaneous stochasticity.

The situations with non-vanishing fluxes through the walls are, however, essentially different. From a mathematical point of view, the problem is 'loss of compactness'. While the trajectories of the reflected diffusion process satisfy uniformly in ν, κ the condition that $\tilde{\boldsymbol{\xi}}_{t,s}^{\nu,\kappa}(\boldsymbol{x}) \in \bar{\Omega}$, a closed, bounded domain, the local-time densities $\tilde{\ell}_{t,s}^{\nu,\kappa}(\boldsymbol{x})$ may become unboundedly large as $\nu, \kappa \to 0$. This creates a fundamental difficulty for arguments of the type employed previously, where limits as $\nu, \kappa \to 0$ were guaranteed to exist (along subsequences). To understand better the problem, consider how we might try to adapt those arguments to the present context. We can rewrite our FDR (2.13) and (2.11) as

$$
\begin{aligned}
\kappa \int_0^t \mathrm{d}s \langle |\boldsymbol{\nabla}\theta(s)|^2 \rangle_\Omega &= \frac{1}{2} \langle \mathrm{Var}[\tilde{\theta}^{\nu,\kappa}(t)] \rangle_\Omega \\
&= \frac{1}{2} \left\langle \int \mathrm{d}\psi \int \mathrm{d}\psi' \; \psi\psi' \; [p_2^{\nu,\kappa}(\psi, \psi'|\cdot, t) - p^{\nu,\kappa}(\psi|\cdot, t)p^{\nu,\kappa}(\psi|\cdot, t)] \right\rangle_\Omega, \quad (2.21)
\end{aligned}
$$

where

$$
p^{\nu,\kappa}(\psi|\boldsymbol{x}, t) = \mathbb{E}[\delta(\psi - \tilde{\theta}^{\nu,\kappa}(\boldsymbol{x}, t))] \quad (2.22)
$$

and

$$
p_2^{\nu,\kappa}(\psi, \psi'|\boldsymbol{x}, t) = \mathbb{E}[\delta(\psi - \tilde{\theta}^{\nu,\kappa}(\boldsymbol{x}, t))\delta(\psi' - \tilde{\theta}^{\nu,\kappa}(\boldsymbol{x}, t))] = \delta(\psi - \psi')p^{\nu,\kappa}(\psi|\boldsymbol{x}, t), \quad (2.23)
$$

with $\tilde{\theta}^{\nu,\kappa}(\boldsymbol{x}, t)$ given by (2.11). If weak limits $p^*(\psi|\boldsymbol{x}, t) = w\text{-}\lim_{\nu,\kappa\to 0} p^{\nu,\kappa}(\psi|\boldsymbol{x}, t)$ existed, then arguments of exactly the type given before would show that anomalous dissipation requires non-factorization of p_2^* into $p^* \cdot p^*$ and, hence, spontaneous stochasticity. The reverse argument that spontaneous stochasticity implies anomalous dissipation for passive scalars would also be essentially the same.

Simple examples show, however, that weak limits $p^*(\psi|\boldsymbol{x}, t) = w\text{-}\lim_{\nu,\kappa\to 0} p^{\nu,\kappa}(\psi|\boldsymbol{x}, t)$ may not exist when wall fluxes are not vanishing. Consider the case where $\theta_0 = S \equiv 0$ and the flux into the domain is a space–time constant $g(\boldsymbol{x}, s) = J > 0$. In that case

$$
\tilde{\theta}(\boldsymbol{x}, t) = \int_0^t g(\tilde{\boldsymbol{\xi}}_{t,s}(\boldsymbol{x}), s) \, \hat{\mathrm{d}}\tilde{\ell}_{t,s}(\boldsymbol{x}) = -J\tilde{\ell}_{t,0}(\boldsymbol{x}) \geqslant 0, \quad (2.24)
$$

and the stochastic scalar field for one realization of the Brownian process is proportional by a constant to the local-time density itself. Consider furthermore the simple case of pure heat conduction, where the advecting velocity field also vanishes, $\boldsymbol{u}^\nu \equiv 0$. In this case, the distribution of $\tilde{\ell}_{t,0}(\boldsymbol{x})$ is known analytically in many cases. A very simple example which serves to make our point takes the domain to

be the semi-infinite one-dimensional interval $\Omega = [0, \infty)$ with boundary at 0. In that case, for $x \geqslant 0$

$$p^\kappa(\psi | x, t) = \frac{1}{J}\sqrt{\frac{\kappa}{\pi t}} \exp\left[-\frac{(x + \kappa\psi/J)^2}{4\kappa t}\right] \eta(\psi) + \left[2\Phi_{\kappa,t}(x) - 1\right]\delta(\psi), \qquad (2.25)$$

where $\eta(\psi)$ is the Heaviside step function and

$$\Phi_{\kappa,t}(x) = \frac{1}{\sqrt{4\kappa\pi t}}\int_{-\infty}^{x} dy \ \exp(-y^2/4\kappa t). \qquad (2.26)$$

For details see appendix A.3. It is easy to see mathematically from the above expression that weak limits exist for fixed $x > 0$ and, indeed,

$$w\text{-}\lim_{\kappa \to 0} p^\kappa(\psi | x, t) = \delta(\psi), \quad x > 0. \qquad (2.27)$$

This is also intuitively obvious, because a stochastic particle released at $x > 0$ never makes it to the boundary at 0 when $\kappa \to 0$. However, the distribution $p^\kappa(\psi | 0, t)$ does not converge weakly as $\kappa \to 0$, but (2.25) implies instead that it tends to become uniformly spread on the semi-infinite interval. This also makes sense, because a particle released at 0 should tend to stay there as $\kappa \to 0$ and the local-time density at 0 will diverge (in fact, if we consider the 1-point compactification $[0, \infty]$ of the range $[0, \infty)$ of possible scalar values, then $\lim_{\kappa \to 0} p^\kappa(\psi | 0, t) = \delta_\infty(\psi)$, the delta function at infinity. However, this compactification of the problem does not yield any result on spontaneous stochasticity).

The physical origin of the divergence in this simple example is a scalar boundary layer near $x = 0$. A direct solution of the Neumann problem for the scalar field or integration over the above distribution shows that

$$\theta(x, t) = -J\mathbb{E}[\tilde{\ell}_{t,0}(x)] \sim J\sqrt{\frac{t}{\kappa}}f\left(\frac{x}{\sqrt{\kappa t}}\right) \qquad (2.28)$$

for a suitable scaling function f. See appendix A.1. There is thus a scalar boundary layer of thickness $\sim\sqrt{\kappa t}$ near 0 where the scalar field diverges as $\theta \sim J\sqrt{t/\kappa}$ as $\kappa \to 0$. Because there is a constant flux J into the domain and diffusive transport into the interior vanishes as $\kappa \to 0$, there is a 'pile up' of the scalar near $x = 0$. The scalar dissipation field due to this boundary layer is

$$\varepsilon_\theta(x, t) = \kappa|\partial_x\theta(x, t)|^2 \sim \frac{J^2}{\kappa}\left|f'\left(\frac{x}{\sqrt{\kappa t}}\right)\right|^2, \qquad (2.29)$$

from which one can infer a total scalar dissipation $\propto J^2\sqrt{t/\kappa} \to \infty$ as $\kappa \to 0$. This 'dissipative anomaly' occurs even though there is clearly no spontaneous stochasticity in this simple example with $\boldsymbol{u}^\nu \equiv 0$!

The above example shows that the 'loss of compactness' is not a mere technical mathematical difficulty, but instead that there may no longer be equivalence of spontaneous stochasticity and non-vanishing dissipation. Scalar boundary layers in wall-bounded flow domains with flux through the walls are a new possible source of scalar dissipation that can be non-zero (or even diverging) as $\nu, \kappa \to 0$, quite distinct from the spontaneous stochasticity mechanism. Another perhaps more elementary way

to see the problem posed by wall fluxes is to exploit formula (2.6) for the boundary local time to write

$$
\mathrm{Var}\left[\int_0^t g(\tilde{\boldsymbol{\xi}}_{t,s}(\boldsymbol{x}), s)\,\hat{\mathrm{d}}\tilde{\ell}_{t,s}(\boldsymbol{x})\right]
$$
$$
= \int_0^t \mathrm{d}s \int_0^t \mathrm{d}s' \int \mathrm{d}H^{d-1}(\boldsymbol{z}) \int \mathrm{d}H^{d-1}(\boldsymbol{z}')\ g(\boldsymbol{z}, s)g(\boldsymbol{z}', s')
$$
$$
\times [p_2^{\nu,\kappa}(\boldsymbol{z}, s; \boldsymbol{z}', s'|\boldsymbol{x}, t) - p^{\nu,\kappa}(\boldsymbol{z}, s|\boldsymbol{x}, t)p^{\nu,\kappa}(\boldsymbol{z}', s'|\boldsymbol{x}, t)], \tag{2.30}
$$

where $p_2^{\nu,\kappa}(\boldsymbol{y}, s; \boldsymbol{y}', s'|\boldsymbol{x}, t)$ for $s, s' < t$ is the 2-time transition probability density function with respect to the Lebesgue measure, defined in (2.19). On the face of it, this appears to be quite similar to the analogous formulae for the scalar variance associated with the initial data or internal sources, e.g. (2.18). However, in the variance associated with θ_0 or S, the transition probability densities appear only in the combinations $\mathrm{d}^d y\ \mathrm{d}^d y'\ p_2^{\nu,\kappa}(\boldsymbol{y}, s; \boldsymbol{y}', s'|\boldsymbol{x}, t)$ and $\mathrm{d}^d y\ p^{\nu,\kappa}(\boldsymbol{y}, s|\boldsymbol{x}, t)$, and thus only involve the probability measures themselves and not their densities. Compactness arguments suffice to show that limits of the probability measures and associated integrals exist (along subsequences) as $\nu, \kappa \to 0$. On the other hand, the formula (2.30) involves the probability density function evaluated on the boundary of the domain. Even if the (weak) limit of the particle probability measures have density functions $p_2^*(\boldsymbol{y}, s; \boldsymbol{y}', s'|\boldsymbol{x}, t)$ and $p^*(\boldsymbol{y}, s|\boldsymbol{x}, t)$, they are undefined at the boundary $\partial\Omega$, which is a Lebesgue zero-measure set. In general, the probability density functions will not have pointwise limits as $\nu, \kappa \to 0$ and, in the example of pure diffusion on the half-line discussed above, they diverge when all three points $\boldsymbol{x}, \boldsymbol{y}, \boldsymbol{y}'$ are located on the left boundary at 0!

On the other hand, we can extend all of our results relating spontaneous stochasticity and anomalous scalar dissipation to general choices of wall fluxes, if we make the additional assumption that pointwise limits of densities exist for all $\boldsymbol{x}, \boldsymbol{y}, \boldsymbol{y}' \in \Omega$

$$
\lim_{\nu,\kappa\to 0} p_2^{\nu,\kappa}(\boldsymbol{y}, s; \boldsymbol{y}', s'|\boldsymbol{x}, t) = p_2^*(\boldsymbol{y}, s; \boldsymbol{y}', s'|\boldsymbol{x}, t), \quad \lim_{\nu,\kappa\to 0} p^{\nu,\kappa}(\boldsymbol{y}, s|\boldsymbol{x}, t) = p^*(\boldsymbol{y}, s|\boldsymbol{x}, t),
$$
$$
\tag{2.31a,b}
$$

so that the limit of the variance in (2.30) exists and is given by the formula

$$
\lim_{\nu,\kappa\to 0} \mathrm{Var}\left[\int_0^t g(\tilde{\boldsymbol{\xi}}_{t,s}(\boldsymbol{x}), s)\,\hat{\mathrm{d}}\tilde{\ell}_{t,s}(\boldsymbol{x})\right]
$$
$$
= \int_0^t \mathrm{d}s \int_0^t \mathrm{d}s' \int \mathrm{d}H^{d-1}(\boldsymbol{z}) \int \mathrm{d}H^{d-1}(\boldsymbol{z}')
$$
$$
\times g(\boldsymbol{z}, s)g(\boldsymbol{z}', s')\ [p_2^*(\boldsymbol{z}, s; \boldsymbol{z}', s'|\boldsymbol{x}, t) - p^*(\boldsymbol{z}, s|\boldsymbol{x}, t)p^*(\boldsymbol{z}', s'|\boldsymbol{x}, t)]. \tag{2.32}
$$

This assumption, of course, rules out the presence of scalar boundary layers of the type discussed above. The necessity of spontaneous stochasticity for anomalous scalar dissipation is immediate, because factorization $p_2^*(\boldsymbol{y}, s; \boldsymbol{y}', s'|\boldsymbol{x}, t) = p^*(\boldsymbol{y}, s|\boldsymbol{x}, t)p^*(\boldsymbol{y}', s'|\boldsymbol{x}, t)$ of the limit densities implies that all variances tend to zero. If the scalar is passive, then sufficiency holds as well. Consider, for simplicity, the case of vanishing internal source $S \equiv 0$. As in Part I, § 4 and appendix A, we can make a smooth choice of scalar initial data θ_0 so that the volume average of the limiting variance in (2.18) is strictly positive, whenever non-factorization holds for a positive-measure set of $\boldsymbol{x} \in \Omega$. The limit variance in (2.32) involving the boundary flux g is non-negative

when it exists at all. If the covariance term involving both θ_0 and g is negative, then by taking $\theta_0 \to -\theta_0$ the covariance can be made positive without changing the sign of either of the two variances involving θ_0 and g separately. In this manner, for any possible choice of wall fluxes g, an initial condition θ_0 for the passive scalar advection equation always exists so that scalar dissipation is non-vanishing as $\nu, \kappa \to 0$. The same conclusion holds also for an active scalar, barring a 'conspiracy' in which all Lagrangian particles at time 0 originating from almost every point $x \in \Omega$ at time t are confined to a single isoscalar surface of θ_0 for that x, even when varying over all possible θ_0. It is this unlikely coincidence which must be ruled out by a rigorous proof. In this manner we see that all of our previous conclusions for flows without walls or for zero fluxes at the walls, can be extended to the case of general wall-fluxes g, whenever the stringent assumption (2.31) on pointwise limits is valid.

3. Imposed scalar values at the wall and mixed conditions

In this section we extend our previous results as far as possible to advection–diffusion of scalars in wall-bounded domains with the general mixed Dirichlet–Neumann conditions (1.2), (1.3). It turns out that imposing scalar values (Dirichlet conditions) on even part of the boundary leads to much more essential difficulties than imposing fluxes (Neumann conditions). In particular, the arguments used earlier for deriving a Lagrangian fluctuation–dissipation relation no longer allow us to express the total volume-integrated scalar dissipation in purely Lagrangian terms. Instead, we can derive two distinct FDRs, one relation giving a lower bound on total scalar dissipation in purely Lagrangian terms and another relation of mixed Euler–Lagrangian character for the total scalar dissipation. The inequality relation allows us to deduce that anomalous dissipation can result from spontaneous stochasticity, but not that spontaneous stochasticity is necessary (In fact, we provide an analytical example of pure heat conduction exhibiting a dissipative anomaly due entirely to thin scalar boundary layers (appendix B).). The equality relation is more useful for physical purposes. We thus derive both relations. We first consider the special case of a scalar $\theta(x, t)$ with pure Dirichlet boundary conditions ($\partial \Omega_D = \partial \Omega$):

$$\left.\begin{array}{l} \partial_t \theta + u \cdot \nabla \theta = \kappa \Delta \theta + S \quad \text{for } x \in \Omega, \\ \theta(x, t) = \psi(x, t) \quad \text{for } x \in \partial \Omega, \end{array}\right\} \tag{3.1}$$

for given initial data θ_0, boundary data ψ, and source field $S(x, t)$. Of course, pure Dirichlet conditions are often encountered in practice, e.g. turbulent channel flow with opposite walls held at two fixed temperatures. This special case already presents the essential new difficulties and, after analysing it in detail, we shall briefly comment on modifications required for the general mixed case.

3.1. *Stochastic representation and fluctuation–dissipation relation*

The standard stochastic representation of solutions of the problem (3.1) involves stochastic particles which are stopped at the boundary, contributing a term due to the value maintained at the wall (Keanini 2007; Soner 2007; Oksendal 2013). The stochastic flow may again be defined with reflection at the boundary, governed by the equation (2.2) involving the boundary local time. The new notion is the boundary (first) hitting time or stopping time, which is defined for $x \in \Omega$ by the larger of
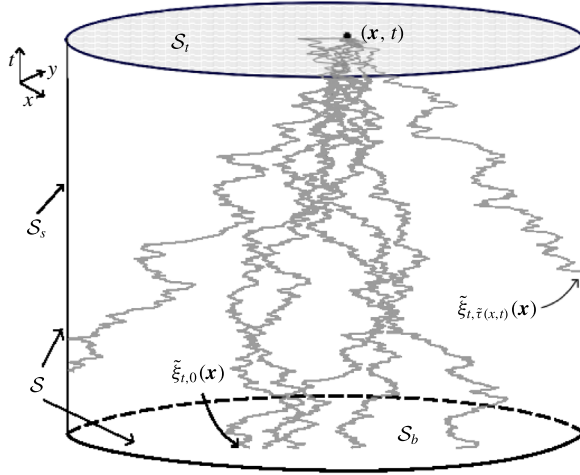
FIGURE 4. A schematic of the space–time domain $\mathcal{D}$ for a disk-shaped space domain $\Omega \subseteq \mathbb{R}^2$, together with realizations of the process $\tilde{\boldsymbol{\xi}}_{t,s}(\boldsymbol{x})$ satisfying (2.2) and stopped at the exit surface $\mathcal{S} = \mathcal{S}_b \cup \mathcal{S}_s$. Some trajectories reach the base $\mathcal{S}_b$ at random points $\tilde{\boldsymbol{\xi}}_{t,0}(\boldsymbol{x})$ whereas others hit the side surface $\mathcal{S}_s$ at points $\tilde{\boldsymbol{\xi}}_{t,\tilde{\tau}(\boldsymbol{x},t)}(\boldsymbol{x})$ and are stopped there.

$\sup\{s : \tilde{\boldsymbol{\xi}}_{t,s}(\boldsymbol{x}) \in \partial\Omega\}$, the first time going in reverse to hit the spatial boundary, and the initial time 0, or

$$\tilde{\tau}(\boldsymbol{x}, t) = \max\{\sup\{s : \tilde{\boldsymbol{\xi}}_{t,s}(\boldsymbol{x}) \in \partial\Omega\}, 0\}. \tag{3.2}$$

This is the first time (going backward) at which the stochastic Lagrangian particle hits the space–time exit surface $\mathcal{S}$, the union of the 'side surface' $\mathcal{S}_s = \partial\Omega \times [0, t)$ and the 'base' $\mathcal{S}_b = \Omega \times \{0\}$ of the right cylindrical domain $\mathcal{D} = \Omega \times [0, t)$ in $(d + 1)$-dimensional space–time, when starting at a point $(\boldsymbol{x}, t)$ in the 'top' $\mathcal{S}_t = \Omega \times \{t\}$. See figure 4.

To state conveniently the stochastic representation, we define the function which gives the data on $\mathcal{S}$:

$$\Theta(\boldsymbol{x}, s) = \begin{cases} \psi(\boldsymbol{x}, s), & s > 0 \text{ and } \boldsymbol{x} \in \partial\Omega \\ \theta_0(\boldsymbol{x}), & s = 0 \text{ and } \boldsymbol{x} \in \Omega. \end{cases} \tag{3.3}$$

Using the backward Itō formula (2.7) and integrating from time t down to the hitting time $\tilde{\tau}(\boldsymbol{x}, t)$ gives

$$\theta(\boldsymbol{x}, t) = \Theta(\tilde{\boldsymbol{\xi}}_{t,\tilde{\tau}(\boldsymbol{x},t)}(\boldsymbol{x}), \tilde{\tau}(\boldsymbol{x}, t)) + \int_{\tilde{\tau}(\boldsymbol{x},t)}^{t} \mathrm{d}t' \; S(\tilde{\boldsymbol{\xi}}_{t,t'}(\boldsymbol{x}), t')$$

$$+ \sqrt{2\kappa} \int_{\tilde{\tau}(\boldsymbol{x},t)}^{t} \hat{\mathrm{d}}\widetilde{\boldsymbol{W}}_{t'} \cdot \nabla\theta(\tilde{\boldsymbol{\xi}}_{t,t'}(\boldsymbol{x}), t'), \tag{3.4}$$

where we used the fact that $\tilde{\ell}_{t,s}(\boldsymbol{x}) \equiv 0$ for all $\tilde{\tau}(\boldsymbol{x}, t) < s < t$ and also used the system (3.1). Taking the expectation over the Brownian motion then yields for solutions of the initial boundary-value problem the following stochastic representation:

$$\theta(\boldsymbol{x}, t) = \mathbb{E}\left[\Theta(\tilde{\boldsymbol{\xi}}_{t,\tilde{\tau}(\boldsymbol{x},t)}(\boldsymbol{x}), \tilde{\tau}(\boldsymbol{x}, t)) + \int_{\tilde{\tau}(\boldsymbol{x},t)}^{t} \mathrm{d}s \; S(\tilde{\boldsymbol{\xi}}_{t,s}(\boldsymbol{x}), s)\right]. \tag{3.5}$$

See Keanini (2007), Soner (2007) and Oksendal (2013) for more details. In particular, the Itō integral in (3.4) is a (backward) martingale by the optional stopping theorem (Oksendal 2013). This formula represents the solution $\theta(\boldsymbol{x}, t)$ to the scalar advection–diffusion equation as an average over randomly sampled sources and initial boundary data.

It is now straightforward to obtain our first version of a fluctuation–dissipation relation by mimicking previous arguments. Applying the Itō isometry valid with the random stopping time as the lower range of the integral (see e.g. Oksendal 2013, Theorem 7.4.1)

$$\mathbb{E}\left|\int_{\tilde{\tau}(\boldsymbol{x},t)}^{t} \hat{\mathrm{d}}\widetilde{\boldsymbol{W}}_s \cdot \boldsymbol{\nabla}\theta(\tilde{\boldsymbol{\xi}}_{t,s}(\boldsymbol{x}), s)\right|^2 = \mathbb{E}\left[\int_{\tilde{\tau}(\boldsymbol{x},t)}^{t} \mathrm{d}s \ |\boldsymbol{\nabla}\theta(\tilde{\boldsymbol{\xi}}_{t,s}(\boldsymbol{x}), s)|^2\right]. \quad (3.6)$$

Thus we obtain from (3.4), (3.5) that

$$\mathrm{Var}\left[\Theta(\tilde{\boldsymbol{\xi}}_{t,\tilde{\tau}(\boldsymbol{x},t)}(\boldsymbol{x}), \tilde{\tau}(\boldsymbol{x}, t)) + \int_{\tilde{\tau}(\boldsymbol{x},t)}^{t} \mathrm{d}s \ S(\tilde{\boldsymbol{\xi}}_{t,s}(\boldsymbol{x}), s)\right]$$
$$= 2\kappa \ \mathbb{E}\left[\int_{\tilde{\tau}(\boldsymbol{x},t)}^{t} \mathrm{d}s \ |\boldsymbol{\nabla}\theta(\tilde{\boldsymbol{\xi}}_{t,s}(\boldsymbol{x}), s)|^2\right]. \quad (3.7)$$

Finally, averaging over the space domain yields

$$\frac{1}{2}\left\langle \mathrm{Var}\left[\Theta(\tilde{\boldsymbol{\xi}}_{t,\tilde{\tau}(t)}, \tilde{\tau}(t)) + \int_{\tilde{\tau}(t)}^{t} \mathrm{d}s \ S(\tilde{\boldsymbol{\xi}}_{t,s}, s)\right]\right\rangle_{\Omega}$$
$$= \kappa \left\langle \mathbb{E}\left[\int_{\tilde{\tau}(t)}^{t} \mathrm{d}s \ |\boldsymbol{\nabla}\theta(\tilde{\boldsymbol{\xi}}_{t,s}, s)|^2\right]\right\rangle_{\Omega}. \quad (3.8)$$

This exact result is one possible version of a fluctuation–dissipation relation for scalar turbulence with general Dirichlet boundary conditions.

Unlike our previous relations, however, the right-hand side of (3.8) above is not the total time-integrated scalar dissipation over the entire domain of the flow. The relation easily yields a lower bound on the total scalar dissipation by simply extending the time integration down to $s = 0$,

$$\frac{1}{2}\left\langle \mathrm{Var}\left[\Theta(\tilde{\boldsymbol{\xi}}_{t,\tilde{\tau}(t)}(\tilde{\tau}(t))) + \int_{\tilde{\tau}(t)}^{t} \mathrm{d}s \ S(\tilde{\boldsymbol{\xi}}_{t,s}, s)\right]\right\rangle_{\Omega} \leqslant \kappa \left\langle \mathbb{E}\left[\int_0^t \mathrm{d}s \ |\boldsymbol{\nabla}\theta(s)|^2\right]\right\rangle_{\Omega}, \quad (3.9)$$

because the s-integrand is non-negative and the reflected stochastic flow is volume preserving, so that the Jacobian of the change of variables from $\tilde{\boldsymbol{\xi}}_{t,s}(\boldsymbol{x})$ to $\boldsymbol{x}$ is unity. The difference between the right-hand and left-hand sides is

$$\Delta^{\nu,\kappa}(t) \equiv \kappa \int_0^t \mathrm{d}s \frac{1}{|\Omega|} \int_{\Omega} \mathrm{d}^d x |\boldsymbol{\nabla}\theta(\boldsymbol{x}, s)|^2 - \kappa \ \mathbb{E}\left[\frac{1}{|\Omega|} \int_{\Omega} \mathrm{d}^d x \int_{\tilde{\tau}(\boldsymbol{x},t)}^{t} \mathrm{d}s |\boldsymbol{\nabla}\theta(\tilde{\boldsymbol{\xi}}_{t,s}(\boldsymbol{x}), s)|^2\right]$$
$$= \kappa \int_0^t \mathrm{d}s \ \mathbb{E}\left[\frac{1}{|\Omega|} \int_{\tilde{\Omega}_{t,s}} \mathrm{d}^d x |\boldsymbol{\nabla}\theta(\tilde{\boldsymbol{\xi}}_{t,s}(\boldsymbol{x}), s)|^2\right], \quad (3.10)$$

where

$$\tilde{\Omega}_{t,s} = \{\boldsymbol{x} \in \Omega : \ \tilde{\tau}(\boldsymbol{x}, t) > s\} \quad (3.11)$$

is the set of positions x for which the stochastic particle has already hit the boundary by time s (going backward). The inequality (3.9) thus fails to be an equality because of the missing contributions to total dissipation at positions of reflected particles. We shall discuss further below the sharpness of the inequality (3.9) and whether it should, in a suitable limit, become equality.

3.2. *Numerical results*

To gain further insight, we present now some numerical results on PDFs of hitting times for the channel-flow database. We considered two release points in the buffer layer at height $\Delta y = 10\delta_\tau$ above the bottom wall and at the final time t_f of the database. The wall-parallel positions of the release points are those shown in figure 2, and thus one is in a high-speed streak and the other in a low-speed streak. It turns out that to calculate hitting-time PDFs accurately using N-sample ensembles of particles is quite difficult, because most particles take a very long time to first hit the boundary. For our results presented here, we evolved $N = 14\,336$ samples of stochastic particles solving (2.2) for three Prandtl numbers $Pr = 0.1, 1, 10$ at both release points. Note that hitting times τ satisfying $t_f - \tau \ll \tau_\nu$ and $t_f - \tau \gg \tau_\nu$ are both very rare events which could not be observed even with so many samples. We thus consider here the logarithmic variable $\lambda \equiv \ln((t_f - \tau)/\tau_\nu)$ which is appropriate to typical values and calculate PDFs $p(\lambda|x, t_f)$. The numerical procedures are discussed at length in appendix D.2. Here we just note that the PDFs are obtained up to the largest available $\lambda = \ln(t_f/\tau_\nu) \doteq 7.17$ and down to $\lambda = -1$, but the PDFs at the two extremes contain further errors that are not indicated by the error bars (representing both s.e.m. for N-samples averages and variation with kernel bandwidth). The PDFs for $\lambda < 1.6$ are shifted to the right by approximately $5\,\%$, because our time step $\Delta s \doteq 2 \times 10^{-3}$ cannot fully resolve the smaller hitting times. For $\lambda > 6.5$ the PDFs from kernel density estimates are too small, because of the end point effect due to unavailability of samples for $\lambda > 7.17$. Our numerical procedures show the same deficiencies when applied to pure Brownian motion, but successfully recover the known analytical results for that case in the range $1.6 < \lambda < 6.5$.

We plot in figure 5 the PDFs $p(\lambda|x, t_f)$ for the two choices of x, the left panel corresponding to particles released in a high-speed streak and the right to particles released in a low-speed streak. We also plot for comparison the analytical results for hitting-time PDFs with pure diffusion (see (D 4) of appendix D.2). One can see in figure 5 a very strong effect of the release point on the hitting-time statistics, unlike the situation for the boundary local times accumulated over one flow-through time. At $Pr = 0.1$ and 1, hitting times are clearly larger than those of pure diffusion for release in a high-speed streak and smaller for release in a low-speed streak. This effect is easy to understand, because particles released in a low-speed streak are advected toward the wall backward in time, and those released in a high-speed streak swept away from the wall. This effect is not observed for $Pr = 10$, with hitting times for pure diffusion very obviously shorter than those for advected particles started in both high-speed and low-speed streaks. This occurs presumably because advection alone can never bring a particle to the wall in a finite time (because of the vanishing velocity there) and as diffusivity κ decreases one sees more strongly the effect of fluid advection, which transports the particles away from the wall. One can see in general a strong effect of diffusivity on the hitting times, with smaller values of κ (or larger Pr) leading to larger hitting times backward in time. We shall refer to this property in our discussion below of the sharpness of the inequality (3.9). However, we first exploit this inequality to prove also for Dirichlet boundary conditions that spontaneous stochasticity is sufficient for anomalous dissipation of passive scalars.
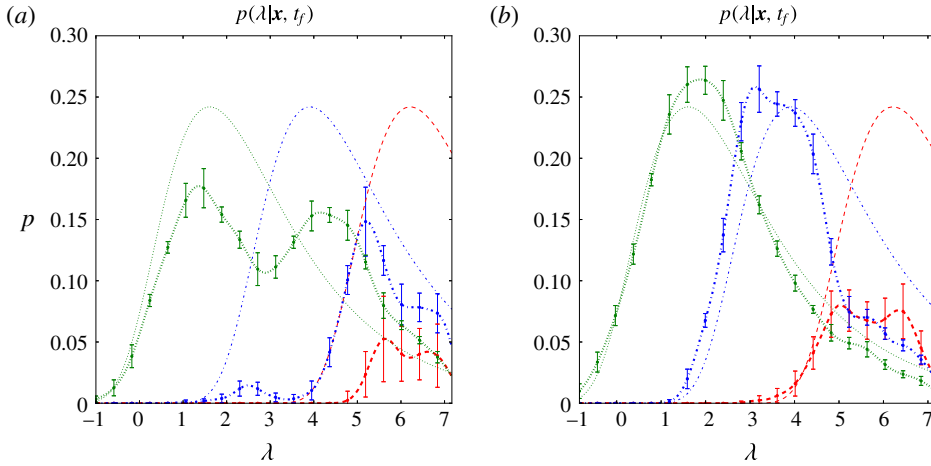
FIGURE 5. (Colour online) PDFs of the logarithmic hitting-time variable $\lambda = \ln((t_f - \tau)/\tau_\nu)$. (*a*) Particles released in a high-speed streak, (*b*) particles released in a low-speed streak, for channel flow (heavy) and pure diffusion (light) for Prandtl numbers $Pr = 0.1$ (green, dot, $\cdots\cdots$), 1.0 (blue, dash-dot, $—\cdot—$) and 10 (red, dash, $----$).

3.3. *Spontaneous stochasticity implies anomalous dissipation*

The argument is very similar to those given earlier. To present it first in the simplest context, we consider a decaying scalar with vanishing source ($S = 0$). We first introduce an analogue of the formula (2.18) for the variance which constitutes the lower bound. There is a natural measure on the exit surface $\mathcal{S}$ (see figure 4) which is just the d-dimensional Hausdorff measure H^d on subsets of $(d + 1)$-dimensional space–time, restricted to $\mathcal{S}$. This can be described in elementary terms using natural d-dimensional coordinates $\boldsymbol{\sigma}$ on $\mathcal{S}$, where on $\mathcal{S}_b$ we have $\boldsymbol{\sigma} = (\boldsymbol{y}, 0)$ for $\boldsymbol{y} \in \Omega$ and on $\mathcal{S}_s$ we have $\boldsymbol{\sigma} = (\boldsymbol{z}, \tau)$ for $\boldsymbol{z} \in \partial\Omega$, the presumed smooth bounding wall surface, and $\tau \in [0, t]$. Then for $\boldsymbol{\sigma} \in \mathcal{S}$

$$H^d(\mathrm{d}\boldsymbol{\sigma}) = \begin{cases} \mathrm{d}^d y & \boldsymbol{\sigma} = (\boldsymbol{y}, 0) \in \mathcal{S}_b \\ \mathrm{d}H^{d-1}(\boldsymbol{z})\mathrm{d}\tau & \boldsymbol{\sigma} = (\boldsymbol{z}, \tau) \in \mathcal{S}_s. \end{cases} \tag{3.12}$$

Here H^{d-1} is the $(d - 1)$-dimensional Hausdorff measure on the smooth wall surface $\partial\Omega$ (that is, the usual $(d - 1)$-dimensional surface area $\mathrm{d}S$). We can then also define the delta distribution $\delta_{\mathcal{S}}(\boldsymbol{\sigma}', \boldsymbol{\sigma})$ on $\mathcal{S}$ with respect to measure H^d, so that

$$\int_{\mathcal{S}} H^d(\mathrm{d}\boldsymbol{\sigma}')f(\boldsymbol{\sigma}')\delta_{\mathcal{S}}(\boldsymbol{\sigma}', \boldsymbol{\sigma}) = f(\boldsymbol{\sigma}) \tag{3.13}$$

for all smooth functions on $\mathcal{S}$, and we can likewise decompose this delta function as

$$\delta_{\mathcal{S}}(\boldsymbol{\sigma}', \boldsymbol{\sigma}) = \begin{cases} \delta^d(\boldsymbol{y}' - \boldsymbol{y}) & \boldsymbol{\sigma}', \boldsymbol{\sigma} \in \mathcal{S}_b \\ \delta_{\partial\Omega}(\boldsymbol{z}', \boldsymbol{z})\delta(\tau' - \tau) & \boldsymbol{\sigma}', \boldsymbol{\sigma} \in \mathcal{S}_s. \end{cases} \tag{3.14}$$

Denoting by $\tilde{\boldsymbol{\sigma}}(\boldsymbol{x}, t) = (\tilde{\boldsymbol{\xi}}_{t, \tilde{\tau}(\boldsymbol{x}, t)}(\boldsymbol{x}), \tilde{\tau}(\boldsymbol{x}, t))$ the space–time point where the trajectory first hits $\mathcal{S}$ (going backward in time), we can then introduce 1-time transition probability

densities for a particle to go backward in time from points $(\boldsymbol{x}, t)$ on the 'top' surface $\Omega \times \{t\}$ of the space–time cylinder and to arrive first to $\mathcal{S}$ at the point $\boldsymbol{\sigma} \in \mathcal{S}$:

$$
\begin{aligned}
q^{\nu,\kappa}(\boldsymbol{\sigma}|\boldsymbol{x}, t) &= \mathbb{E}[\delta_{\mathcal{S}}(\boldsymbol{\sigma}, \tilde{\boldsymbol{\sigma}}(\boldsymbol{x}, t))] \\
&= \begin{cases} \mathbb{E}[\delta^d(\boldsymbol{y} - \tilde{\boldsymbol{\xi}}_{t,0}(\boldsymbol{x}))] & \boldsymbol{\sigma} = (\boldsymbol{y}, 0) \in \mathcal{S}_b \\ \mathbb{E}[\delta_{\partial\Omega}(\boldsymbol{z} - \tilde{\boldsymbol{\xi}}_{t,\tau}(\boldsymbol{x}))\delta(\tau - \tilde{\tau}(\boldsymbol{x}, t))] & \boldsymbol{\sigma} = (\boldsymbol{z}, \tau) \in \mathcal{S}_s. \end{cases}
\end{aligned} \quad (3.15)
$$

This probability density is normalized with respect to H^d on $\mathcal{S}$ so that

$$
\int_{\mathcal{S}} H^d(\mathrm{d}\boldsymbol{\sigma}) q(\boldsymbol{\sigma}|\boldsymbol{x}, t) = 1. \quad (3.16)
$$

In these terms we obtain a simple formula for the stochastic representation (3.5) in the case of vanishing scalar source:

$$
\theta(\boldsymbol{x}, t) = \mathbb{E}[\Theta(\tilde{\boldsymbol{\sigma}}(\boldsymbol{x}, t))] = \int_{\mathcal{S}} H^d(\mathrm{d}\boldsymbol{\sigma}) \; \Theta(\boldsymbol{\sigma}) \; q(\boldsymbol{\sigma}|\boldsymbol{x}, t). \quad (3.17)
$$

We note in passing here that there is another representation for $q(\boldsymbol{\sigma}|\boldsymbol{x}, t)$ in terms of a process of stochastic Lagrangian particles which is distinct from that considered so far. Rather than letting the particles reflect off the wall, one can instead kill the particles when they hit the wall (absorbing boundary conditions). If $k(\boldsymbol{a}, s|\boldsymbol{x}, t)$ for $s < t$ is the transition probability density for this killed process backward in time, then

$$
q(\boldsymbol{\sigma}|\boldsymbol{x}, t) = \begin{cases} k(\boldsymbol{y}, 0|\boldsymbol{x}, t) & \boldsymbol{\sigma} = (\boldsymbol{y}, 0) \in \mathcal{S}_b \\ \boldsymbol{\mu}(\boldsymbol{z}, \tau) \cdot \nabla_{\boldsymbol{z}} k(\boldsymbol{z}, \tau|\boldsymbol{x}, t) & \boldsymbol{\sigma} = (\boldsymbol{z}, \tau) \in \mathcal{S}_s. \end{cases} \quad (3.18)
$$

Here we make use of the general connection between the joint density function of the hitting time and location and between the normal derivative of the transition probability for the killed process; see Freĭdlin (1985) and Hsu (1986). This alternative stochastic interpretation will prove useful for calculations in appendix B.

We can obtain a similar formula as (3.17) for the variance, if we introduce also the corresponding twofold transition probabilities

$$
q_2^{\nu,\kappa}(\boldsymbol{\sigma}, \boldsymbol{\sigma}'|\boldsymbol{x}, t) = \mathbb{E}[\delta_{\mathcal{S}}(\boldsymbol{\sigma}, \tilde{\boldsymbol{\sigma}}(\boldsymbol{x}, t))\delta_{\mathcal{S}}(\boldsymbol{\sigma}', \tilde{\boldsymbol{\sigma}}(\boldsymbol{x}, t))] = \delta_{\mathcal{S}}(\boldsymbol{\sigma}, \boldsymbol{\sigma}') q(\boldsymbol{\sigma}|\boldsymbol{x}, t), \quad (3.19)
$$

so that

$$
\begin{aligned}
\mathrm{Var}[\Theta(\tilde{\boldsymbol{\sigma}}(\boldsymbol{x}, t))] = \int_{\mathcal{S}} H^d(\mathrm{d}\boldsymbol{\sigma}) \int_{\mathcal{S}} H^d(\mathrm{d}\boldsymbol{\sigma}') \; &\Theta(\boldsymbol{\sigma})\Theta(\boldsymbol{\sigma}') \\
\times \; &[q_2(\boldsymbol{\sigma}, \boldsymbol{\sigma}'|\boldsymbol{x}, t) - q(\boldsymbol{\sigma}|\boldsymbol{x}, t) q(\boldsymbol{\sigma}'|\boldsymbol{x}, t)].
\end{aligned} \quad (3.20)
$$

These results are formally identical to those for the sourceless ($S = 0$) scalar in domains without boundary or with zero-flux Neumann conditions at the wall. Furthermore, $\mathcal{S}$ is a compact subset of space–time. Thus, we can exactly mimic our previous arguments with no change. Limits q^*, q_2^* as $\nu_j, \kappa_j \to 0$ always exist along suitable subsequences ν_j, κ_j. If the limits were deterministic, then one would have

$$
q_2^*(\boldsymbol{\sigma}, \boldsymbol{\sigma}'|\boldsymbol{x}, t) = q^*(\boldsymbol{\sigma}|\boldsymbol{x}, t) q^*(\boldsymbol{\sigma}'|\boldsymbol{x}, t) \quad (3.21)
$$

so that q_2^* would factorize in a product of two q^* values. However, if the limits are non-deterministic so that q_2^* does not factorize for a positive-measure set of $\boldsymbol{x}$ at time t, then there must be some smooth choice of $\Theta = (\theta_0, \psi)$ that makes the non-negative space-averaged variance in (3.20) in fact non-zero. For such choice of initial condition θ_0 and boundary conditions ψ, the space-averaged and time-integrated scalar dissipation will then be non-zero taking the limit $v_j, \kappa_j \to 0$. As before, this argument works rigorously only for a passive scalar, not an active one. An additional limitation discussed further in appendix C is that we cannot use this argument to prove, for a fixed choice of the boundary data ψ, that spontaneous stochasticity implies there exists a smooth initial datum θ_0 for which the scalar dissipation rate is positive (These comments have implications for the problem of Rayleigh–Bénard convection with fixed temperatures at top/bottom plates, which is discussed in Part III. There is some evidence for Richardson dispersion of Lagrangian particles in numerical simulations of turbulent convection (Schumacher 2008). However, even if there were compelling evidence for spontaneous stochasticity associated with this effect, we could not rigorously conclude from our results that there is anomalous thermal dissipation. First, the temperature is an active scalar in that case and, second, our present arguments do not work with fixed boundary data). Minor changes to these arguments are needed to incorporate a bulk source S and we leave details also to appendix C.

The previous arguments do not imply that spontaneous stochasticity is required for anomalous scalar dissipation with imposed scalar values at the wall. Even if the factorization (3.21) holds and there is no spontaneous stochasticity, the variance in (3.20) provides only a lower bound to the scalar dissipation. Hence, the scalar dissipation rate can tend to a non-zero limit even when the variance vanishes! This is not just a failure of the proof, but also an indication that other physical mechanisms are available to produce anomalous dissipation with Dirichlet boundary conditions. The most obvious alternative mechanism is a narrow scalar boundary layer at the walls. One can imagine a flow with extremely rapid advective mixing in the interior and with opposite scalar values $\pm\psi_0$ imposed at two ends, so that large scalar gradients of the order $\nabla\theta \sim O(\psi_0/\kappa)$ are achieved in a boundary layer of thickness $\sim O(\kappa)$ and a near-zero scalar amplitude $\theta \simeq 0$ occurs over the bulk of the domain. Such a flow would be the simplest that provides anomalous scalar dissipation from a scalar boundary-layer mechanism. For example, one might consider a fluid undergoing solid-body rotation with frequency ω in the interior of the domain and an imposed inhomogeneous temperature distribution on the boundary varying between $-\psi_0$ and $+\psi_0$. In the rotating frame of reference, this would correspond to a motionless fluid (pure heat conduction) but with a time-dependent boundary temperature oscillating with frequency ω between the extreme values $\pm\psi_0$.

As the simplest example of this type, consider pure diffusion on the interval $[0, H]$ with $\theta_0 = S \equiv 0$ and boundary temperatures specified as $\psi(0, t) = \psi_0 \sin(\omega t)$ and $\psi(H, t) = 0$. In this case, the stochastic scalar field is simply

$$\tilde{\theta}(\boldsymbol{x}, t) = \psi_0 \sin(\omega \tilde{\tau}(x, t)). \tag{3.22}$$

The scalar field $\theta(x, t) = \mathbb{E}[\tilde{\theta}(\boldsymbol{x}, t)]$ can be constructed with the knowledge of the hitting-time distribution at zero for Brownian motion on the half-line, which is

$$p^\kappa(\tau | x, t) = \begin{cases} \dfrac{x}{\sqrt{4\pi\kappa(t-\tau)^3}} \exp\left(-\dfrac{x^2}{4\kappa(t-\tau)}\right) & \tau < t \\ 0 & \tau > t. \end{cases} \tag{3.23}$$

See appendix B. The solution $\theta(x, t)$ of the conduction problem can be obtained by integration over the above distribution, and scalar gradients can then be explicitly computed; see (B 23). Temperature fluctuations are found to propagate with velocity $(\kappa\omega)^{1/2}$ and travel to distances $(\kappa/\omega)^{1/2}$ away from the wall. In this small boundary-layer region, the scalar field gradients diverge as $\partial_x\theta \sim \psi_0(\omega/\kappa)^{1/2}$ as $\kappa \to 0$. We obtain

$$\int_0^L \mathrm{d}x \; \kappa |\partial_x\theta(x, t)|^2 \propto (\kappa/\omega)^{1/2} \cdot \kappa \cdot \psi_0^2(\omega/\kappa) \sim \psi_0^2\sqrt{\kappa\omega}. \tag{3.24}$$

See (B 14) for a more precise statement. The scalar field in this simple example exhibits anomalous dissipation if ω is very large for $\kappa \to 0$, e.g. with $\omega \sim \kappa^{-\alpha}$ for $\alpha \geqslant 1$. In particular, for $\alpha = 1$ the limiting scalar dissipation rate is non-zero and finite as $\kappa \to 0$, with scalar gradients and boundary-layer thicknesses as suggested in the previous paragraph. Thus, just as for flux boundary conditions, thin scalar boundary layers can be a source of non-zero (possibly diverging) dissipation as $\nu, \kappa \to 0$.

3.4. *Equality fluctuation–dissipation relation*

We now return to the question whether our lower bound (3.9) on the cumulative (time- and space-integrated) scalar dissipation may in fact be an equality. This is certainly not true in the $t \to \infty$ limit with κ, ν fixed. We note that

$$\lim_{t\to\infty} \tilde{\Omega}_{t,s} = \Omega, \quad \text{any fixed } s > 0 \tag{3.25}$$

since the boundary hitting times are finite almost surely for $\kappa, \nu > 0$ (see Karlin & Taylor 1981, chap. 15, § 11) and, thus, the particle released in the far distant future t will certainly hit the space boundary $\partial\Omega$ before s (moving backward in time). Thence by dominated convergence

$$\lim_{t\to\infty} \mathbb{E}\left[\int_{\tilde{\xi}_{t,s}(\tilde{\Omega}_{t,s})} \mathrm{d}^d x \; \kappa \; |\nabla\theta(\boldsymbol{x}, s)|^2\right] = \kappa \int_{\Omega} \mathrm{d}^d x \; |\nabla\theta(\boldsymbol{x}, s)|^2 \tag{3.26}$$

and the contribution of reflected particles coincides at long times with the total dissipation. A strengthened conclusion is that

$$\lim_{t\to\infty} \tilde{\Omega}_{t,s} = \Omega, \quad \text{uniformly for all } s \text{ such that } t - \delta(t) \geqslant s \geqslant 0, \tag{3.27}$$

for some function $\delta(t) \geqslant 0$ such that $\lim_{t\to\infty} \delta(t) = \infty$, $\lim_{t\to\infty} \delta(t)/t = 0$. This is true because the difference $t - s \geqslant \delta(t)$ for all such s. In that case, however, we see that

$$\lim_{t\to\infty} \frac{1}{t}\Delta^{\nu,\kappa}(t) = \lim_{t\to\infty} \frac{1}{t}\int_0^t \mathrm{d}s \; \frac{1}{|\Omega|}\int_{\Omega} \mathrm{d}^d x \, \kappa |\nabla\theta(\boldsymbol{x}, s)|^2, \tag{3.28}$$

where $\Delta^{\nu,\kappa}(t)$ is the difference in (3.10). Thus, our lower bound (3.9) on space–time average dissipation becomes vacuous as $t \to \infty$, with the long-time limit of the lower bound simply tending to zero as reflected particles fill the entire domain.

Now consider the opposite limit with $\nu, \kappa \to 0$ for fixed t. If we keep ν fixed so that the velocity stays smooth, then no particles will reach the boundary in the finite time interval $[0, t]$ as $\kappa \to 0$. An increase of hitting times with decreasing κ for fixed ν is clearly observed in figure 5. In this limit, the inequality in our lower bound

becomes equality. However, as long as $\boldsymbol{u}$ is smooth, then there will be no dissipative anomaly and the scalar dissipation will vanish! Thus, this limit is of little interest. On the other hand, if we take $\nu, \kappa \to 0$ together, then it is possible that the particles will hit the boundary and reflect. In fact, this must be the case if there is a scalar dissipative anomaly at finite times t for flux boundary conditions and vanishing initial data of the scalar and vanishing scalar sources, since then the FDR (2.13) is solely due to the contribution of the boundary local times in (2.11). If particles continue to hit the boundary as $\nu, \kappa \to 0$ for fixed time t, then our lower bound must be a strict inequality (but possibly non-vanishing for finite t).

It is straightforward, however, to obtain an equality relation for the scalar dissipation by using the same derivation as for flux boundary conditions, namely, by using the backwards Itō formula (2.7) and integrating from time t down to 0, rather than stopping when hitting the boundary. This argument yields for the scalar itself

$$\theta(\boldsymbol{x}, t) = \mathbb{E}\left[\theta_0(\tilde{\boldsymbol{\xi}}_{t,0}(\boldsymbol{x})) + \int_0^t \mathrm{d}s \ S(\tilde{\boldsymbol{\xi}}_{t,s}(\boldsymbol{x}), s) - \kappa \int_0^t \boldsymbol{\mu} \cdot \boldsymbol{\nabla}\theta(\tilde{\boldsymbol{\xi}}_{t,s}(\boldsymbol{x}), s) \, \hat{\mathrm{d}}\tilde{\ell}_{t,s}(\boldsymbol{x})\right] \quad (3.29)$$

and for the variance

$$\frac{1}{2}\left\langle \mathrm{Var}\left[\theta_0(\tilde{\boldsymbol{\xi}}_{t,0}) + \int_0^t \mathrm{d}s \ S(\tilde{\boldsymbol{\xi}}_{t,s}, s) - \kappa \int_0^t \boldsymbol{\mu} \cdot \boldsymbol{\nabla}\theta(\tilde{\boldsymbol{\xi}}_{t,s}(\boldsymbol{x}), s) \, \hat{\mathrm{d}}\tilde{\ell}_{t,s}\right]\right\rangle_\Omega$$
$$= \kappa \int_0^t \mathrm{d}s \left\langle |\boldsymbol{\nabla}\theta(s)|^2 \right\rangle_\Omega, \quad (3.30)$$

which is our second version of a fluctuation–dissipation relation for Dirichlet boundary conditions of the scalar. The total scalar dissipation is now obtained, with the contribution of the reflected particles represented by the boundary local-time density term on the left. Unfortunately, this new formula is not very convenient for mathematical analysis, because the scalar boundary flux $g(\boldsymbol{x}, t) = -\boldsymbol{\mu} \cdot \boldsymbol{\nabla}\theta(\boldsymbol{x}, t)$ is no longer a known input, but is instead a space–time fluctuating quantity which must be determined from the solution of the scalar advection–diffusion equation. This relation thus has a mixed Euler–Lagrangian character, because it involves both the Eulerian scalar field $\theta(\boldsymbol{x}, t)$ and the stochastic Lagrangian flow $\tilde{\boldsymbol{\xi}}_{t,s}$. Despite being clumsy for mathematical use, this relation is the physically most natural version of the FDR for scalar Dirichlet boundary conditions, and provides insight into the Lagrangian origin of scalar dissipation. In appendix B.2, we explicitly demonstrate the equivalence of the formula (3.29) to the more standard representation (3.17) for the simple example of heat conduction with oscillating wall temperature.

3.5. *Mixed boundary conditions*

The extension of the previous results to scalars with general mixed Dirichlet–Neumann conditions (1.2), (1.3) is straightforward. Again, one considers the backward stochastic flow with reflection at the boundary. To derive an FDR in the form of an inequality like (3.8), one must stop those particles which hit $\partial\Omega_D$ before time 0 (going backward). The particles which hit $\partial\Omega_N$ are simply reflected. Results like (3.7) and (3.8) are obtained, except that now the stopping time $\tilde{\tau}(\boldsymbol{x}, t)$ is the first time to hit $\partial\Omega_D$ (or 0, whichever is larger) and the variance on the left includes contributions from the local-time density at the piece $\partial\Omega_N$ of the boundary. This FDR inequality omits the contribution to scalar dissipation at locations of particles reflected from $\partial\Omega_D$.

It is also easy to obtain an FDR equality like (3.30) by stopping no particles. It has an identical form to (3.30) and the sole difference is that $g(\boldsymbol{x}, t) = -\boldsymbol{\mu} \cdot \nabla \theta(\boldsymbol{x}, t)$ is a specified function for points $\boldsymbol{x} \in \partial \Omega_N$ but must be obtained for $\boldsymbol{x} \in \partial \Omega_D$ by solving the advection–diffusion equation. We shall make use of this version of the FDR in our discussion of turbulent Rayleigh–Bénard convection in the following Part III.

4. Summary and discussion

This paper has extended to flows in wall-bounded domains the Lagrangian fluctuation–dissipation relation introduced in Part I for scalars advected by an incompressible fluid. This relation expresses an exact balance between molecular dissipation of the scalar and input of scalar variance from the initial values, boundary fluxes and internal sources as these are sampled by stochastic Lagrangian trajectories backward in time. We have exploited this relation to prove, for domains with no scalar flux through the wall, that spontaneous stochasticity of Lagrangian trajectories is necessary and sufficient for anomalous dissipation of passive scalars, and necessary (but possibly not sufficient) for anomalous dissipation of active scalars. Cream stirred into coffee is an everyday example of this type, as is any scalar advected by a fluid in a container with impermeable walls. For more general mixed boundary conditions on the scalar, with imposed values at the wall or imposed non-zero fluxes, simple examples show that thin scalar boundary layers provide a distinct mechanism for non-vanishing scalar dissipation. Nevertheless, we can still show rigorously for general scalar boundary conditions that spontaneous stochasticity is sufficient for anomalous dissipation of passive scalars, and this result plausibly extends to active scalars as well. Thus, in addition to scalar boundary layers, Lagrangian spontaneous stochasticity is shown here to be another possible source of anomalous scalar dissipation in wall-bounded flows.

An interesting issue for further study is whether Lagrangian spontaneous stochasticity plays any role in anomalous dissipation of kinetic energy in wall-bounded flows. There is some evidence from experimental measurements of turbulence in closed containers that, while the kinetic energy dissipation due to viscous boundary layers decreases very slowly with increasing Reynolds number, the energy dissipation in the bulk of the turbulent flow is very nearly Reynolds number independent (Cadot *et al.* 1997). It appears possible that such 'anomalous dissipation' in the bulk is produced by very similar mechanisms as energy dissipation in homogeneous, isotropic turbulence and thus may be related to spontaneous stochasticity in the bulk, as discussed in Part I. Note that the stochastic Lagrangian representation of incompressible Navier–Stokes solutions discussed in Part I has been successfully extended to wall-bounded flows with stick boundary conditions for the velocity at the wall (Constantin & Iyer 2011). The Lagrangian dynamics of vorticity in this stochastic formulation generalizes the classical Helmholtz theorem for ideal Euler solutions. Indeed, similar to the case of scalar fields with Dirichlet conditions discussed in §3, the vorticity field at a point is an average of 'frozen-in' vorticity vectors that are transported along an ensemble of stochastic Lagrangian trajectories backward in time. Those trajectories that hit the wall transport the vorticity that they encounter there, while those that never hit the wall before time 0 transport the initial vorticity. See Constantin & Iyer (2011) for detailed discussion and proofs. These results make it possible to study in detail the contribution of Lagrangian vorticity dynamics, e.g. stretching of vortex filaments, to turbulent energy dissipation in wall-bounded flows. A crucial difference from homogeneous, isotropic turbulence, however, is that random stretching dynamics is

insufficient to explain energy dissipation in the presence of walls, but instead vortex lines generated at the wall must undergo organized motion away from the wall (Taylor 1932; Huggins 1970; Eyink 2008). We therefore expect that the effects of walls on Lagrangian mechanisms of turbulent energy dissipation are quite profound.

The Lagrangian fluctuation–dissipation relation proved in the present paper is valid in wall-bounded flows for all scalars, passive or active, whether either Lagrangian spontaneous stochasticity or scalar anomalous dissipation occur or not in a particular flow. In general, the FDR provides a novel Lagrangian view of turbulent scalar dissipation. In the following Part III we apply the FDR derived here to turbulent Rayleigh–Bénard convection, where the mean thermal dissipation rate and the mean kinetic energy dissipation rate are closely related to each other and also to the vertical heat transport through the convection cell. In Rayleigh–Bénard turbulence it is well known that dissipative anomalies for kinetic energy and thermal fluctuations, if they exist, lead to an 'ultimate regime' of convection at high Rayleigh numbers, with scaling of the heat flux as predicted by Spiegel (1971) or, with a logarithmic correction, by Kraichnan (1962). The absence of dissipative anomalies instead leads to a weaker dependence of heat flux on Rayleigh number than predicted by the Kraichnan–Spiegel theories. Exploiting our Lagrangian FDRs (2.13) and (3.30) we are able to relate the thermal dissipation rate in Rayleigh–Bénard turbulence to the integral mixing time required for passive tracers released at the top or bottom wall to attain to their final uniform value near those walls. We conclude from our analysis that dissipative anomalies and Kraichnan–Spiegel scaling will hold, unless this near-wall mixing time is asymptotically much longer than the gravitational free-fall time or, nearly, the large-scale circulation time. This concrete application thus provides a wider window into the Lagrangian mechanisms of turbulent dissipation.

Acknowledgements

Appendix A. Heat conduction with imposed fluxes

As an illustration of the general formalism and also as basis of comparison for advected scalars, we consider here the Neumann problem for the diffusion equation on the interval $[0, H]$, with imposed fluxes at the end points. As in the main text, we adopt the terminology of heat conduction and thus consider the scalar to be temperature. We work out explicit analytical results for the stochastic representation and fluctuation–dissipation relation in the limit $\kappa \to 0$ at any fixed time t.

The problem considered is stated precisely as

$$\left.\begin{array}{ll} \partial_t T = \kappa \, \partial_x^2 T & \text{for } x \in [0, H] \\ \kappa \, \partial_x T = -J & \text{at } x = 0, H \\ T = 0 & \text{at } t = 0. \end{array}\right\} \tag{A 1}$$

The scalar flux J at the boundaries is a space–time constant and also independent of κ. The Green's function for the problem (A 1) or, equivalently, the transition probability density of the reflected Brownian motion, satisfies, for all $t > 0$ and $x \in [0, H]$, the backward evolution equation:

$$\left. \begin{array}{rl} \partial_s p(a, s|x, t) = -\kappa \partial_a^2 p(a, s|x, t) & \text{for } (a, s) \in [0, H] \times [0, t] \\ \partial_a p(a, s|x, t) = 0 & \text{at } a = 0, H \\ p(a, t|x, t) = \delta(a - x). & \end{array} \right\} \tag{A 2}$$

The solution to (A 2) can be represented using Fourier cosine series:

$$p(a, s|x, t) = \frac{1}{H} + \frac{2}{H} \sum_{n=1}^{\infty} \cos\left(\frac{n\pi}{H}x\right) \cos\left(\frac{n\pi}{H}a\right) e^{-\kappa(n\pi/H)^2(t-s)}. \tag{A 3}$$

A.1. *Temperature profile and boundary layer*

The temperature field can be represented via mean boundary local times at $x = 0$ and $x = H$ using the general stochastic representation formula (2.9):

$$T(x, t) = -J(\mathbb{E}\tilde{\ell}_{t,0}^0(x) - \mathbb{E}\tilde{\ell}_{t,0}^H(x)) = J \int_0^t \mathrm{d}s \, (p(0, s|x, t) - p(H, s|x, t)) . \tag{A 4}$$

We first study the limiting profile $T(x, t)$ as $\kappa \to 0$ via the stochastic representation (A 4). In the coarsest sense, this limit can be obtained from the convergence of the mean local times to delta distributions at the boundary. Indeed, integrating against an arbitrary smooth test function $\varphi \in C^\infty[0, H]$ satisfying $\varphi'(0) = \varphi'(H) = 0$, we have, using the representation (A 3):

$$-\int_0^H \mathrm{d}x \, \varphi(x) \, \mathbb{E}\tilde{\ell}_{t,0}^{\sigma H}(x) = a_0 t + \frac{H^2}{\kappa \pi^2} \sum_{n=1}^{\infty} \frac{(-1)^{n\sigma}}{n^2} (1 - e^{-\kappa(n\pi/H)^2 t}) a_n, \tag{A 5}$$

where $\sigma = 0, 1$ and

$$a_0 = \frac{1}{H} \int_0^H \varphi(x) \, \mathrm{d}x, \quad a_n = \frac{2}{H} \int_0^H \varphi(x) \cos\left(\frac{n\pi}{H}x\right) \mathrm{d}x. \tag{A 6a,b}$$

Because the Fourier coefficients a_n are rapidly decaying in n for smooth φ, the series is absolutely convergent and the $\kappa \to 0$ limit yields

$$\lim_{\kappa \to 0} \int_0^H \mathrm{d}x \, \varphi(x) \, \left(-\mathbb{E}\tilde{\ell}_{t,0}^{\sigma H}(x)\right) = t \left[a_0 + \sum_{n=1}^{\infty} (-1)^{n\sigma} a_n\right] = t\varphi(\sigma H), \tag{A 7}$$

where we have used $\varphi(x) = a_0 + \sum_{n=1}^{\infty} a_n \cos((n\pi)/Hx)$. Therefore we find

$$-\lim_{\kappa \to 0} \mathbb{E}[\tilde{\ell}_{t,0}^0(x)] = t\delta(x), \quad -\lim_{\kappa \to 0} \mathbb{E}[\tilde{\ell}_{t,0}^H(x)] = t\delta(x - H), \tag{A 8a,b}$$

in the sense of distributions and thus

$$\lim_{\kappa \to 0} T(x, t) = Jt(\delta(x) - \delta(x - H)) \tag{A 9}$$

in the sense of distributions.

These delta functions represent thin thermal boundary layers for small values of $\kappa > 0$. The small-κ asymptotics can be inferred by rewriting the transition density (A 3) as

$$
\begin{aligned}
&p(a, s|x, t) \\
&= \frac{1}{H} \sum_{n=-\infty}^{\infty} \cos\left(\frac{n\pi}{H}x\right) \cos\left(\frac{n\pi}{H}a\right) e^{-\kappa(n\pi/H)^2(t-s)} \\
&= \frac{1}{\sqrt{4\kappa\pi(t-s)}} \sum_{n=-\infty}^{\infty} \left(\exp\left(-\frac{(x-a+2nH)^2}{4\kappa(t-s)}\right) + \exp\left(-\frac{(x+a+2nH)^2}{4\kappa(t-s)}\right) \right),
\end{aligned}
$$

(A 10)

where we have employed the Poisson summation formula (see e.g. Katznelson 2004) in passing to the second equality. This is a useful reformulation since series (A 10) is rapidly convergent for $\kappa(t-s)/H^2 \ll 1$ whereas (A 3) converges rapidly for $\kappa(t-s)/H^2 \gg 1$. Thus, at fixed t and H we can study the zero-diffusion limit $\kappa \to 0$ directly from this formula. In particular, since $x, a \in [0, H]$, the asymptotic transition probability is

$$
\begin{aligned}
p(a, s|x, t) \sim\ & \frac{1}{\sqrt{4\kappa\pi(t-s)}} \left(\exp\left(-\frac{(x-a)^2}{4\kappa(t-s)}\right) + \exp\left(-\frac{(x+a)^2}{4\kappa(t-s)}\right) \right. \\
& \left. + \exp\left(-\frac{(x+a-2H)^2}{4\kappa(t-s)}\right) \right) \quad \text{as } \kappa \to 0.
\end{aligned}
$$

(A 11)

All other terms in the sum (A 10) vanish transcendentally. In fact, for $0 \leqslant a, x \ll H$ only two terms remain,

$$
p(a, s|x, t) \sim \frac{1}{\sqrt{4\kappa\pi(t-s)}} \left(\exp\left(-\frac{(x-a)^2}{4\kappa(t-s)}\right) + \exp\left(-\frac{(x+a)^2}{4\kappa(t-s)}\right) \right) \quad \text{as } \kappa \to 0,
$$

(A 12)

which may be recognized as the transition probability for the diffusion process $\tilde{X}(s) = |x + \sqrt{2\kappa}\tilde{W}(t-s)|$ on the half-line $[0, \infty)$, which is a (scaled) Brownian process starting at x at time t moving backward in time s and reflected at the origin. This result is intuitively clear, since the right boundary of the interval at H should play no role for $a, x \ll H$ in the limit $\kappa \to 0$ at fixed times. By the exact symmetry $p(H-a, s|H-x, t) = p(a, s|x, t)$, there is a similar asymptotics with only two terms surviving in (A 11) for a, x near H. We shall thus restrict our asymptotic analysis of the thermal boundary layer to that near $x = 0$, and infer the result near $x = H$ by symmetry.

We introduce a scaled coordinate $\xi = x/\sqrt{\kappa t}$ which is held fixed as $\kappa \to 0$. From the mean value $-\mathbb{E}\tilde{\ell}_{t,0}^0(x) = \int_0^t \mathrm{d}s\, p(0, s|x, t)$ and (A 12) one easily obtains that

$$
-\mathbb{E}\tilde{\ell}_{t,0}^0\left(\sqrt{\kappa t}\xi\right) \sim \left(\frac{t}{\kappa}\right)^{1/2} f(\xi), \quad \text{as } \kappa \to 0, \text{ with } f(\xi) = \frac{1}{\sqrt{\pi}} \int_0^1 \frac{\mathrm{d}u}{\sqrt{u}} \exp\left(-\frac{\xi^2}{4u}\right).
$$

(A 13)

The scaling function $f(\xi)$ satisfies $f(0) = 2/\sqrt{\pi}$, $\int_0^\infty \mathrm{d}\xi\, f(\xi) = 1$, and vanishes rapidly for $\xi \gg 1$. The mean of the boundary local time $\tilde{\ell}_{t,0}^0(x)$ vanishes transcendentally for

x in the interior $(0, H)$ of the domain, but the convergence is highly non-uniform. In particular, at points within a distance $\sqrt{\kappa t}$ of the walls, the mean local times are of order $\sqrt{t/\kappa}$. We immediately conclude for the temperature field that

$$T(x, t) \sim J \left(\frac{t}{\kappa}\right)^{1/2} \left[f\left(\frac{x}{\sqrt{\kappa t}}\right) - f\left(\frac{H-x}{\sqrt{\kappa t}}\right)\right] \tag{A 14}$$

when $\kappa \ll H^2/t$. This asymptotics refines the earlier result (A 9). Without the aid of the diffusivity to spread it, the temperature rises unboundedly at the walls as $\kappa \to 0$.

We can use the above asymptotics to study also the temperature gradient and the scalar dissipation. Indeed, by differentiating the formula (A 14) and using $f'(\xi) = -\text{erfc}(\xi/2)$ in terms of the complementary error function, we obtain

$$\partial_x T(x, t) \sim -\frac{J}{\kappa} \left[\text{erfc}\left(\frac{x}{\sqrt{4\kappa t}}\right) + \text{erfc}\left(\frac{H-x}{\sqrt{4\kappa t}}\right)\right] \tag{A 15}$$

for $\kappa \ll H^2/t$. This clearly satisfies the flux boundary conditions in (A 1). We can exploit this formula to evaluate the space–time average of the thermal dissipation field $\varepsilon_T(x, t) = \kappa |\partial_x T(x, t)|^2$ in the limit $\kappa \to 0$. Using the improper integral $\int_0^\infty \text{erfc}^2(z) \, dz = 1/\sqrt{\pi}(2 - \sqrt{2})$ (Ng & Geller 1969), it is straightforward to show that

$$\langle \varepsilon_T \rangle_{V,t} \equiv \frac{1}{t} \int_0^t ds \frac{1}{H} \int_0^H dx \, \kappa |\partial_x T(x, s)|^2 \sim \frac{8}{3\sqrt{\pi}}(2 - \sqrt{2})\frac{J^2}{H}\sqrt{\frac{t}{\kappa}}. \tag{A 16}$$

Apart from the precise numerical prefactor, this is the scaling that one would expect for temperature gradients of magnitude $\partial_x T \sim J/\kappa$ in a boundary layer of thickness $\sim \sqrt{\kappa t}$.

A.2. *Fluctuation–dissipation relation*

We calculate next the variance in our local FDR (2.12) for the problem (A 1):

$$\langle \varepsilon_T^{fluc}(x) \rangle_t = \frac{J^2}{2t} \text{Var}[(\tilde{\ell}_{t,0}^L(x) - \tilde{\ell}_{t,0}^R(x))]. \tag{A 17}$$

This 'fluctuational dissipation' has the same average over space as the time-averaged molecular dissipation $1/t \int_0^t ds \, \varepsilon_T(x, s)$ and the two quantities are presumably spatially well correlated at short times. To evaluate the space average of (A 17), we employ the general formula (2.30) to write

$$\langle \varepsilon_T^{fluc} \rangle_{V,t} = \frac{2J^2}{H} \int_0^H dx \frac{1}{t} \int_0^t ds \int_s^t ds'$$
$$\times ([p(0, s|0, s') - p(0, s|x, t)] - [p(H, s|0, s') - p(H, s|x, t)])p(0, s'|x, t). \tag{A 18}$$

Here we have used the symmetry of the integral in s, s' and the backward Markov property of the transition probabilities. We have also made use of the $0 \leftrightarrow H$ symmetry after integrating over $[0, H]$. Using the asymptotics (A 11), we have for any $x \in [0, H]$, keeping only the leading terms:

$$[p(H, s|0, s') - p(H, s|x, s')]p(0, s'|x, t)$$

$$\sim \left[\frac{\exp\left(-\dfrac{H^2}{4\kappa(t-s)}\right)}{\sqrt{4\kappa\pi(s'-s)}} - \frac{\exp\left(-\dfrac{(x-H)^2}{4\kappa(t-s)}\right)}{\sqrt{4\kappa\pi(t-s)}} \right] \left[\frac{\exp\left(-\dfrac{x^2}{4\kappa(t-s')}\right)}{\sqrt{4\kappa\pi(t-s')}} \right]$$

$$\longrightarrow 0 \text{ transcendentally}, \quad \text{as } \kappa \to 0. \tag{A 19}$$

Thus, all heterohedral terms vanish as $\kappa \to 0$ and only homohedral terms contribute to the scalar variance. Because of our use of the $0 \leftrightarrow H$ symmetry, only the contributions from $\langle \varepsilon_T^{fluc}(x) \rangle_t$ for $0 \leqslant x \ll H$ survive (multiplied by 2), where as $\kappa \to 0$

$$\langle \varepsilon_T^{fluc}((\kappa t)^{1/2}\xi) \rangle_t \sim \frac{J^2}{t} \int_0^t \mathrm{d}s \int_s^t \mathrm{d}s' [p(0, s|0, s') - p(0, s|\sqrt{\kappa t}\,\xi, t)]p(0, s'|\sqrt{\kappa t}\,\xi, t)$$

$$\sim \frac{J^2}{\kappa\pi t} \int_0^t \mathrm{d}s \int_s^t \mathrm{d}s' \left[\frac{\exp\left(-\dfrac{\xi^2 t}{4(t-s')}\right)}{\sqrt{(s'-s)(t-s')}} - \frac{\exp\left(-\dfrac{\xi^2 t(2t-s-s')}{4(t-s)(t-s')}\right)}{\sqrt{(t-s)(t-s')}} \right]. \tag{A 20}$$

Integrating over ξ from 0 to ∞ and multiplying by $2/H$ gives, after a change of variables to $u = s/t$, $u' = s'/t$,

$$\langle \varepsilon_T^{fluc} \rangle_{V,t} \sim \frac{2}{\sqrt{\pi}} \frac{J^2}{H} \left(\frac{t}{\kappa}\right)^{1/2} \int_0^1 \mathrm{d}u \int_u^1 \mathrm{d}u' \left[\frac{1}{\sqrt{u'-u}} - \frac{1}{\sqrt{2-(u+u')}} \right]. \tag{A 21}$$

The double integral is easily reduced to elementary integrals, with the value $4/3(2 - \sqrt{2})$. Thus, we obtain finally

$$\langle \varepsilon_T^{fluc} \rangle_{V,t} \sim \frac{8}{3\sqrt{\pi}}(2 - \sqrt{2})\frac{J^2}{H}\sqrt{\frac{t}{\kappa}}, \quad \kappa \to 0, \tag{A 22}$$

in exact agreement with (A 16).

The local dissipation measures $\langle \varepsilon_T^{fluc}(x) \rangle_t$ and $\langle \varepsilon_T(x) \rangle_t$ need not be the same pointwise, but they should be closely correlated. To test this idea for pure heat conduction, we have numerically evaluated the x-integrand in (A 18) after re-symmetrization under the reflection $x \leftrightarrow H - x$, by using the analytical representation (A 10) of the transition probabilities truncated to a finite number of terms. The double time integral in (A 18) was evaluated using the Matlab function `integral2`, setting absolute tolerance `abstol=1e-10` and relative tolerance `reltol=1e-8`. In figure 6 we plot the resulting local scalar variance $\langle \varepsilon_T^{fluc}(x) \rangle_t$ using the three-term expansion (A 11), but we have verified that adding further terms from the full expansion (A 10) made no observable change. We also plot for comparison the local dissipation $\langle \varepsilon_T(x) \rangle_t$ obtained from the asymptotic temperature gradient (A 15). Though not identical, we see a close qualitative correspondence of the spatial behaviour of these two dissipation measures, particularly for small dimensionless time $\tau \equiv \kappa t/H^2$ when the dissipation accumulates at the walls.
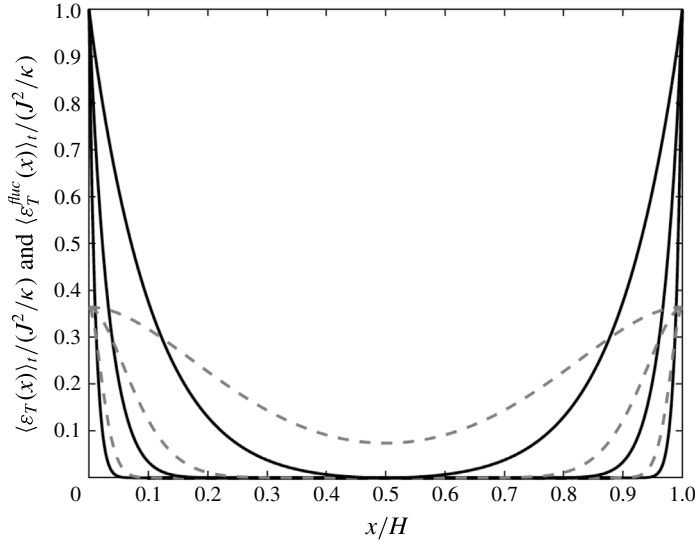
FIGURE 6. Local thermal dissipation (black, solid) and scalar variance (grey, dashed) for pure heat conduction on a one-dimensional interval, non-dimensionalized by J^2/κ, plotted for three dimensionless times $\tau \equiv \kappa t/H^2 = 5 \times 10^{-2}, \ 5 \times 10^{-3}, \ 5 \times 10^{-4}$. The dissipation and variance both localize near the walls as τ decreases.

A.3. *Boundary local-time density of reflected Brownian on the half-line*

The formula (2.25) invoked in § 2.3 is a standard result for a Brownian motion on the half-line $(0, \infty)$ reflected at 0, at least forward in time. Since the Wiener process is time reversible, the formula holds also backward in time. However, even forward in time we could find no reference which gave the result (2.25) for general values of diffusivity $\kappa > 0$. Thus, we here very succinctly review the standard arguments which lead to (2.25), with references to more detailed discussions.

If $\tilde{B}(t)$ is a standard Brownian motion (Wiener process), then the Brownian motion with diffusivity κ started at $x \geqslant 0$ and reflected at 0 is given by the simple formula

$$\tilde{X}(t) = |\sqrt{2\kappa}\tilde{B}(t) - x|. \tag{A 23}$$

Note that $\tilde{B}(t)$ has units of (time)$^{1/2}$ whereas $\tilde{X}(t)$ has units of (length). The evolution of $\tilde{X}(t)$ can be obtained from the Tanaka equation for $a \geqslant 0$:

$$\begin{aligned} |\tilde{B}(t) - a| &= a + \int_0^t \mathrm{sign}(\tilde{B}(t) - a)\,\mathrm{d}\tilde{B}(t) + \int_0^t \mathrm{d}s\ \delta(\tilde{B}(s) - a) \\ &= a + \tilde{W}(t) + \tilde{L}_t(a), \end{aligned} \tag{A 24}$$

where $\tilde{W}(t) = \int_0^t \mathrm{sign}(\tilde{B}(t) - a)\,\mathrm{d}\tilde{B}(t)$ is another standard Brownian motion and $\tilde{L}_t(a)$ is the local time of $\tilde{B}(t)$ at point a. For these well-known results, see Karatzas & Shreve (1991, § 3.6) and Rogers & Williams (2000, §§ IV.6.43–44). (Possibly confusingly, there are different normalizations of local time in the literature, as discussed by Karatzas & Shreve (1991, Remark 3.6.4) and Rogers & Williams (2000, Remark IV.6.43.12). We follow the conventions of the latter.) Setting $a = x/\sqrt{2\kappa}$ in

the Tanaka equation and multiplying through by $\sqrt{2\kappa}$ gives

$$
\begin{aligned}
\tilde{X}(t) &= x + \sqrt{2\kappa}\tilde{W}(t) + \kappa \int_0^t \mathrm{d}s \ \delta(\tilde{X}(s)) \\
&= x + \sqrt{2\kappa}\tilde{W}(t) + \kappa\tilde{\ell}_{0,t}(x).
\end{aligned}
\tag{A 25}
$$

We used here that $\delta(\tilde{X}(t) - \epsilon) = \delta(\sqrt{2\kappa}\tilde{B}(t) - x - \epsilon) + \delta(\sqrt{2\kappa}\tilde{B}(t) - x + \epsilon)$ for any $\epsilon > 0$, in order to relate the local times of $\tilde{B}(t)$ and $\tilde{X}(t)$. See Rogers & Williams (2000, p. 101) and Karatzas & Shreve (1991, Remark 3.7.4). We have also used our normalization convention for the boundary local-time density $\tilde{\ell}_{0,t}(x)$, which does not incorporate the factor of κ into the definition of the local-time density.

We next note the expression for the boundary local-time density given by the Skorohod equation

$$
\kappa\tilde{\ell}_{0,t}(x) = \max\left\{0, \sup_{0\leqslant s\leqslant t}(-x - \sqrt{2\kappa}\tilde{W}(s))\right\}.
\tag{A 26}
$$

See Karatzas & Shreve (1991, Lemma 3.6.14). Define $\tilde{W}_-(t) = -\tilde{W}(t)$, which is another standard Brownian motion, and denote its maximum up to time t by $\tilde{M}(t) = \sup_{0\leqslant s\leqslant t}\tilde{W}_-(s)$, so that

$$
\kappa\tilde{\ell}_{0,t}(x) = \max\{0, -x + \sqrt{2\kappa}\tilde{M}(t)\}.
\tag{A 27}
$$

It is well known (and easy to see) that if $\tilde{\tau}(z)$ is the time for $\tilde{W}_-(t)$ to first hit z, then

$$
P(\tilde{M}(t) > z) = P(\tilde{\tau}(z) < t).
\tag{A 28}
$$

The latter probability can be evaluated by the reflection principle:

$$
P(\tilde{\tau}(z) < t) = 2P(\tilde{W}_-(t) > z).
\tag{A 29}
$$

See Karatzas & Shreve (1991, § 2.6). Thus, for $z > 0$,

$$
P(\tilde{M}(t) < z) = 2P(\tilde{W}_-(t) < z) - 1 = 2\Phi_t(z) - 1,
\tag{A 30}
$$

with

$$
\Phi_t(z) = \frac{1}{\sqrt{2\pi t}} \int_{-\infty}^z \mathrm{d}y \ \exp(-y^2/2t).
\tag{A 31}
$$

Using this result and (A 27) gives

$$
P(\tilde{\ell}_{0,t}(x) < \ell) =
\begin{cases}
2\Phi_t\left(\dfrac{x + \kappa\ell}{\sqrt{2\kappa}}\right) - 1 & \text{for } \ell > 05 \\
0 & \text{for } \ell < 0.
\end{cases}
\tag{A 32}
$$

Finally, differentiating with respect to ℓ gives (2.25) in the main text.

Appendix B. Heat conduction with oscillating temperature boundary conditions

We consider here consider the heat equation on the interval $[0, H]$ with an oscillating temperature imposed at the left end point. We work out explicit analytical results for both stochastic representations (3.17)–(3.18) and (3.29), and briefly discuss the fluctuation–dissipation relation (3.30) in the limit $\kappa \to 0$ at any fixed time t.

The problem considered is stated precisely as

$$\left.\begin{aligned}
\partial_t T &= \kappa \partial_x^2 T \quad \text{for } x \in [0, H], \\
T &= \sin(\omega t) \quad \text{at } x = 0, \\
T &= 0 \quad \text{at } x = H, \\
T &= 0 \quad \text{at } t = 0.
\end{aligned}\right\} \tag{B 1}$$

Here T is made dimensionless by division with ψ_0, so that the maximum value at the boundary $x = 0$ is unity. The Green's function for the problem (B 1) or, equivalently, the transition probability density of killed Brownian motion (absorbing boundaries), satisfies, for all $t > 0$ and $x \in [0, H]$, the backward evolution equation:

$$\left.\begin{aligned}
\partial_s k(a, s|x, t) &= -\kappa \partial_a^2 k(a, s|x, t) \quad \text{for } (a, s) \in [0, H] \times [0, t] \\
k(a, s|x, t) &= 0 \quad \text{at } a = 0, H \\
k(a, t|x, t) &= \delta(a - x).
\end{aligned}\right\} \tag{B 2}$$

The solution to (B 2) can be represented using Fourier sine series:

$$k(a, s; x, t) = \frac{2}{H} \sum_{n=1}^{\infty} \sin\left(\frac{n\pi x}{H}\right) \sin\left(\frac{n\pi a}{H}\right) e^{-\kappa(n\pi/L)^2 (t-s)} \tag{B 3}$$

$$= \frac{1}{\sqrt{4\pi\kappa t}} \sum_{n=-\infty}^{\infty} \left(\exp\left(-\frac{(x - a + 2nH)^2}{4\kappa t}\right) - \exp\left(-\frac{(x + a + 2nH)^2}{4\kappa t}\right) \right). \tag{B 4}$$

The sum (B 3) converges rapidly for large $|t - s|$ whereas the second (B 4), obtained by an application of the Poisson summation formula, converges rapidly for small κ. We employ the latter form for subsequent analysis in this section.

B.1. *Temperature profile and boundary layer*

According to the Feynman–Kac formula (3.17)–(3.18), the temperature is represented by

$$T(x, t) = \kappa \int_0^t \mathrm{d}s \; \sin(\omega s) \left[\frac{\partial}{\partial a} k(a, s; x, t)\right]_{a=0}, \tag{B 5}$$

where the probability flux through the boundary

$$\kappa \left[\frac{\partial}{\partial a} k(a, s; x, t)\right]_{a=0} = \frac{1}{\sqrt{4\pi\kappa(t-s)^3}} \sum_{n=-\infty}^{\infty} (x + 2nL) \exp\left(-\frac{(x + 2nL)^2}{4\kappa(t-s)}\right). \tag{B 6}$$

This can be interpreted as the probability distribution function for the first hitting time at the left boundary of Brownian motion on the finite interval $[0, H]$ starting at (x, t) (see Hsu 1986). As $\kappa \to 0$ at fixed t, all terms in (B 6) vanish transcendentally except

$$\kappa \left[\frac{\partial}{\partial a} k(a, s; x, t) \right]_{a=0} \sim \frac{x}{\sqrt{4\pi\kappa (t-s)^3}} e^{-x^2/4\kappa(t-s)} \quad \text{as } \kappa \to 0. \tag{B 7}$$

Formula (B 7) is identified as the first boundary hitting-time density function for Brownian motion on the half-line $[0, \infty)$, equation (3.23). This well-known result (Karatzas & Shreve 1991, § 2.6) can be obtained by differentiating $P(\tilde{\tau}(z) < t)$ in (A 29) with respect to t and setting $t \to t - s$. As a result, the temperature is given by

$$T(x, t) \sim \frac{x}{\sqrt{4\pi\kappa}} \int_0^t \mathrm{d}s \, \frac{\sin(\omega s)}{(t-s)^{3/2}} e^{-x^2/4\kappa(t-s)} \quad \text{as } \kappa \to 0. \tag{B 8}$$

This is the exact solution to the heat equation on the half-line $[0, \infty)$ with the oscillating boundary conditions at $x = 0$ in (B 1). It follows from (B 8) that, with x, t fixed, $T(x, t) \to 0$ as $\kappa \to 0$. In that limit the temperature field is non-vanishing only in a thin boundary layer.

To analyse behaviour in this layer, we introduce the scaling variable $\xi = x\sqrt{\omega/\kappa}$ and a dimensionless time $\beta = \omega(t - s)$ so that

$$T(\xi, t) \sim \frac{\xi}{2\sqrt{\pi}} \int_0^{\omega t} \mathrm{d}\beta \, \frac{\sin(\omega t - \beta)}{\beta^{3/2}} e^{-\xi^2/4\beta}. \tag{B 9}$$

Since the integral (B 9) is absolutely convergent at $\beta = \infty$, we can divide it into two pieces, $T(\xi, t) = T_{qs}(\xi, t) + T_{tr}(\xi, t)$, the first with the upper integration range extended to infinity

$$T_{qs}(\xi, t) = \frac{\xi}{2\sqrt{\pi}} \int_0^{\infty} \mathrm{d}\beta \, \frac{\sin(\omega t - \beta)}{\beta^{3/2}} e^{-\xi^2/4\beta} \tag{B 10}$$

and the complementary piece

$$T_{tr}(\xi, t) = -\frac{\xi}{2\sqrt{\pi}} \int_{\omega t}^{\infty} \mathrm{d}\beta \, \frac{\sin(\omega t - \beta)}{\beta^{3/2}} e^{-\xi^2/4\beta}, \tag{B 11}$$

which tends to zero as $t \to \infty$. The first term (B 10) represents quasi-steady conduction with long-time oscillation of the temperature at the frequency ω imposed by the boundary conditions, while the second term (B 11) describes the transient heating-up phase that results from a uniformly cold, semi-infinite 'rod' being exposed suddenly to a periodic temperature variation at its end. The quasi-stationary part can be evaluated explicitly by a standard Laplace transform (Erdélyi 1954, 4.5(28), p. 146)

$$\int_0^{\infty} \mathrm{d}\beta \, \beta^{-3/2} \exp\left(-\sigma\beta - \alpha/4\beta\right) = 2\left(\frac{\pi}{\alpha}\right)^{1/2} \exp(-\sqrt{\sigma\alpha}), \quad \mathrm{Re}(\sigma) \geqslant 0, \quad \mathrm{Re}(\alpha) > 0, \tag{B 12a-c}$$

implying, with $\alpha = \xi^2$, $\sigma = \mathrm{i}$ and $\sqrt{\mathrm{i}} = (1 + \mathrm{i})/\sqrt{2}$, that

$$T_{qs}(\xi, t) = e^{-\xi/\sqrt{2}} \sin(\omega t - \xi/\sqrt{2}). \tag{B 13}$$

The thermal dissipation in the scaled variables is given by

$$\langle \varepsilon_T \rangle_{V,t} \equiv \frac{1}{t} \int_0^t \mathrm{d}s \, \frac{1}{H} \int_0^H \mathrm{d}x \, \kappa |\partial_x T(x, s)|^2$$

$$= \sqrt{\omega \kappa} \cdot \frac{1}{t} \int_0^t \mathrm{d}s \, \frac{1}{H} \int_0^{H(\omega/\kappa)^{1/2}} \mathrm{d}\xi |\partial_\xi T(\xi, s)|^2. \tag{B 14}$$

In the limit $\kappa \to 0$, the upper range $H(\omega/\kappa)^{1/2}$ of the ξ-integral can be set to infinity, since the integrand decays rapidly to zero as $\xi \to \infty$. This is equivalent to the statement that the thermal dissipation occurs entirely within the narrow temperature boundary layer of thickness $\sim (\kappa/\omega)^{1/2}$. The quasi-steady contribution due to (B 13) is found from

$$\partial_\xi T_{qs}(\xi, t) = -\mathrm{e}^{-\xi/\sqrt{2}} \sin\left(\omega t - \xi/\sqrt{2} + \frac{\pi}{4}\right) \tag{B 15}$$

and

$$\frac{1}{t} \int_0^t \mathrm{d}s \int_0^\infty \mathrm{d}\xi |\partial_\xi T_{qs}(\xi, s)|^2 = \frac{1}{2\sqrt{2}} - \frac{\cos(2\omega t) - 1}{2\omega t} \frac{1}{4\sqrt{2}} - \frac{\sin(2\omega t)}{2\omega t} \frac{1}{4\sqrt{2}}. \tag{B 16}$$

To evaluate the contribution from the transient, we use the derivative of (B 11)

$$\partial_\xi T_{tr}(\xi, t) = -\frac{1}{2\sqrt{\pi}} \int_{\omega t}^\infty \mathrm{d}\beta \, \frac{\sin(\omega t - \beta)}{\beta^{3/2}} \left(1 - \frac{\xi^2}{2\beta}\right) \mathrm{e}^{-\xi^2/4\beta}, \tag{B 17}$$

which is again an absolutely convergent integral. Substituting this integral and performing the Gaussian integrals over ξ, one easily finds that

$$\int_0^\infty \mathrm{d}\xi |\partial_\xi T_{tr}(\xi, t)|^2 = \frac{3}{4}\sqrt{\pi} \int_{\omega t}^\infty \mathrm{d}\beta_1 \, \sin(\omega t - \beta_1) \int_{\omega t}^\infty \mathrm{d}\beta_2 \, \sin(\omega t - \beta_2) \frac{1}{(\beta_1 + \beta_2)^{5/2}}$$

$$\leqslant \frac{3}{4}\left(\frac{\pi}{\omega t}\right)^{1/2} \int_1^\infty \mathrm{d}u_1 \int_1^\infty \mathrm{d}u_2 \frac{1}{(u_1 + u_2)^{5/2}} = \left(\frac{\pi}{2\omega t}\right)^{1/2}, \tag{B 18}$$

which provides an $O(1/\sqrt{\omega t})$ correction to the quasi-stationary result. Likewise, the cross-term between the quasi-stationary and transient parts is

$$2 \int_0^\infty \mathrm{d}\xi \, \partial_\xi T_{qs}(\xi, t) \partial_\xi T_{tr}(\xi, t)$$

$$= \frac{1}{\sqrt{\pi}} \int_{\omega t}^\infty \frac{\mathrm{d}\beta}{\beta^{3/2}} \sin(\omega t - \beta) \int_0^\infty \mathrm{d}\xi \, \sin\left(\omega t - \frac{\xi}{\sqrt{2}} + \frac{\pi}{4}\right) \left(1 - \frac{\xi^2}{2\beta}\right) \mathrm{e}^{-\xi/\sqrt{2} - \xi^2/4\beta}, \tag{B 19}$$

which is bounded by

$$\left| 2 \int_0^\infty \mathrm{d}\xi \, \partial_\xi T_{qs}(\xi, t) \partial_\xi T_{tr}(\xi, t) \right| \leqslant \frac{1}{\sqrt{\pi}} \int_{\omega t}^\infty \frac{\mathrm{d}\beta}{\beta^{3/2}} \int_0^\infty \mathrm{d}\xi \, \left(1 + \frac{\xi^2}{2\beta}\right) \mathrm{e}^{-\xi/\sqrt{2}}$$

$$= 2\left(\frac{2}{\pi\omega t}\right)^{1/2} \left(1 + \frac{2}{3\omega t}\right). \tag{B 20}$$
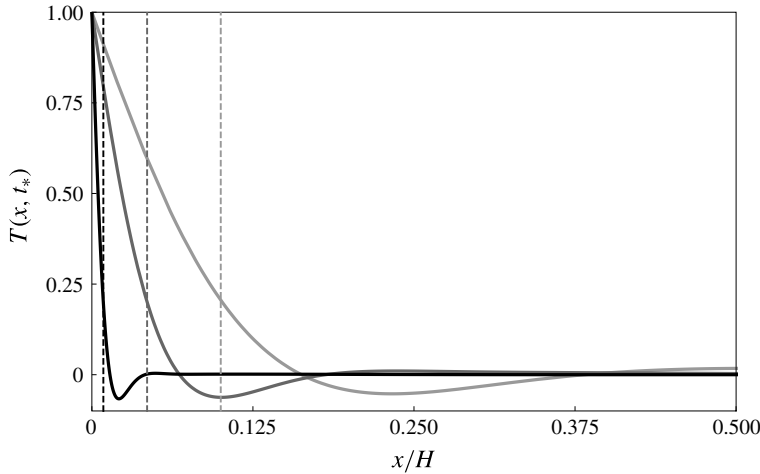
FIGURE 7. Temperature distribution for pure conduction on a one-dimensional interval with oscillating Dirichlet boundary conditions, depicted at a fixed instant t_* such that $t_*\sqrt{\omega\kappa}/H = 1$. Plotted are solutions for three pairs of (ω, κ) satisfying $(\omega t_*)(\kappa t_*/H^2) = 1$; these are $\omega t_* = 9\pi/2$ (light grey), $\omega t_* = 21\pi/2$ (grey) and $\omega t_* = 101\pi/2$ (black). The dashed vertical lines, which indicate the boundary-layer region, are placed at $(2\kappa/\omega)^{1/2}$.

Gathering all these results together,

$$\langle \varepsilon_T \rangle_{V,t} = \frac{\psi_0^2 \sqrt{\omega\kappa}}{2\sqrt{2}H} \left[1 + O\left(\frac{1}{\sqrt{\omega t}} \right) \right], \tag{B 21}$$

with the leading contribution coming from time average of the quasi-steady term. Here we have restored the factor ψ_0^2 from the amplitude of the oscillating boundary temperature.

Apart from the numerical pre-factor, this result could have been expected on dimensional grounds; see (3.24) of §3.3. In order to obtain a result non-vanishing in the limit $\kappa \to 0$, the frequency ω must go to infinity and, in that case, the time-dependent corrections all vanish. Assuming that $\omega \sim \kappa^{-\alpha}$ as $\kappa \to 0$, we have

$$\left. \begin{aligned} 0 \leqslant \alpha < 1 \quad &\text{then} \quad \lim_{\kappa \to 0} \langle \varepsilon_T \rangle_{V,t} = 0, \\ \alpha = 1 \quad &\text{then} \quad \lim_{\kappa \to 0} \langle \varepsilon_T \rangle_{V,t} = (\text{const.}), \\ \alpha > 1 \quad &\text{then} \quad \lim_{\kappa \to 0} \langle \varepsilon_T \rangle_{V,t} = +\infty. \end{aligned} \right\} \tag{B 22}$$

Note that $\omega \sim \kappa^{-1}$ illustrates the scenario described in §3.3 since the temperature gradients have magnitude $\partial_x T \sim 1/\kappa$ in a boundary layer of thickness $(\kappa/\omega)^{1/2} \sim \kappa$. See figure 7 for plot of steepening profile (B 8), indicating temperature gradients growing unboundedly large in the boundary layer as $\kappa \to 0$, $\omega = \kappa^{-1} \to \infty$.

B.2. *Alternative Feynman–Kac formula and fluctuation–dissipation relation*

In §3.4 of the main body of the text, we showed that there are two equivalent stochastic representations valid for scalars supplied with Dirichlet boundary conditions. One of these representations involves first hitting times (3.18) and the other involves

local-time integrals (3.29). The utility of the former representation (3.18) was demonstrated in the previous subsection where it was used to explicitly solve the heat equation (B 9). The latter formula (3.29) is also theoretically useful as it allows us to obtain an FDR equality for Dirichlet boundary conditions (see (3.30) of § 3.4). On the other hand, the formula (3.29) is computationally unwieldy since it requires sampling the (*a priori* unknown) flux $g(x, t) := \kappa \partial_x T(x, t)$ at the boundary with reflecting (not killed) Brownian motion. Here, as a consistency check, we demonstrate the equivalence of these formulae directly for conduction on the semi-infinite space interval $(0, \infty)$ with oscillating boundary condition at $x = 0$.

A formula for the flux follows by direct differentiation of (B 8), which yields

$$
\begin{aligned}
g(x, t) &= -\sqrt{\frac{\kappa}{\pi}} \int_0^t \mathrm{d}s \frac{\sin(\omega s)}{(t-s)^{3/2}} \frac{1}{2} \left(1 - \frac{x^2}{2\kappa(t-s)} \right) \mathrm{e}^{-x^2/4\kappa(t-s)} \\
&= -\sqrt{\frac{\kappa}{\pi}} \int_0^t \mathrm{d}s \sin(\omega s) \frac{\partial}{\partial s} \left[\frac{\mathrm{e}^{-x^2/4\kappa(t-s)}}{(t-s)^{1/2}} \right] \\
&= \omega \sqrt{\frac{\kappa}{\pi}} \int_0^t \mathrm{d}s \frac{\cos(\omega s)}{(t-s)^{1/2}} \exp\left(-\frac{x^2}{4\kappa(t-s)} \right),
\end{aligned}
\tag{B 23}
$$

after an integration by parts. Thus, the temperature profile according to the local-time representation (3.29) is given by

$$
\begin{aligned}
T(x, t) &= \int_0^t \mathrm{d}s \ g(0, s) p(0, s|x, t) \\
&= \frac{\omega}{\pi} \int_0^t \mathrm{d}s \int_0^s \mathrm{d}s' \frac{\cos(\omega s')}{\sqrt{s-s'}\sqrt{t-s}} \exp\left(-\frac{x^2}{4\kappa(t-s)} \right),
\end{aligned}
\tag{B 24}
$$

where we have used the transition density for reflecting Brownian motion (A 12). Interchanging the order of the integrals,

$$
T(x, t) = \frac{\omega}{\pi} \int_0^t \mathrm{d}s' \cos(\omega s') \int_{s'}^t \mathrm{d}s \frac{\exp\left(-\dfrac{x^2}{4\kappa(t-s)} \right)}{\sqrt{s-s'}\sqrt{t-s}}.
\tag{B 25}
$$

Under the substitutions $u = x^2/4\kappa(t-s)$ and $b = x^2/4\kappa(t-s')$ the inner integral becomes

$$
\int_{s'}^t \mathrm{d}s \frac{\exp\left(-\dfrac{x^2}{4\kappa(t-s)} \right)}{\sqrt{s-s'}\sqrt{t-s}} = \sqrt{b} \int_b^\infty \mathrm{d}u \frac{\mathrm{e}^{-u}}{(u-b)^{1/2}u} = \pi \ \mathrm{erfc}(\sqrt{b}),
\tag{B 26}
$$

in terms of the complementary error function erfc(z), by Erdélyi (1954, 4.2(26), p. 136). The local-time representation formula (B 25) therefore gives

$$
T(x, t) = \omega \int_0^t \mathrm{d}s' \ \cos(\omega s') \ \mathrm{erfc}\left(\frac{x}{\sqrt{4\kappa(t-s')}} \right).
\tag{B 27}
$$

Using the expression (B 27) and $\omega \cos(\omega s') = (\partial/\partial s') \sin(\omega s')$, a straightforward integration by parts in s' recovers the formula (B 8) from the hitting-time representation.

Thus, the two stochastic representations are verified to yield identical results for this problem.

Additionally, as we did in appendix A.2 for the case of temperature supplied with Neumann conditions, one can verify directly that the second form (3.30) of our fluctuation–dissipation relation equals the total dissipation (B 14). The FDR (3.30) for the present problem on the space interval $(0, H)$ reduces asymptotically as $\kappa \to 0$ to

$$
\begin{aligned}
\langle \varepsilon_T^{fluc}(x) \rangle_{V,t} &= \frac{1}{H} \int_0^H \mathrm{d}x \, \frac{1}{2} \mathrm{Var} \left[\int_0^t \kappa \, \partial_x T(\tilde{\xi}_{t,s}(x), s) \, \hat{\mathrm{d}} \tilde{\ell}_{t,s}^L(x) \right] \\
&= \frac{1}{H} \int_0^H \mathrm{d}x \int_0^t \mathrm{d}s \int_s^t \mathrm{d}s' g(0, s) g(0, s') [p(0, s|0, s') - p(0, s|x, t)] p(0, s'|x, t),
\end{aligned}
$$
(B 28)

where, again, the fluxes $g(0, t)$ are explicitly defined by (B 23). A straightforward but lengthy calculation, similar to the one we performed to show the equivalence of the two Feynman–Kac representations, verifies that one obtains the same asymptotic expression for the dissipation (B 14) directly from our exact fluctuation–dissipation relation.

Appendix C. Spontaneous stochasticity implies anomalous scalar dissipation for Dirichlet scalar boundary conditions

We supply here details of the proofs in §3.3 that spontaneous stochasticity implies anomalous dissipation of a passive scalar with appropriate choices of initial data, Dirichlet boundary data and bulk scalar sources. For active scalars, it seems likely that this remains true but, due to lack of freedom in choosing the scalar data, we cannot rigorously draw such conclusions.

C.1. *Vanishing scalar sources*

For zero scalar sources, we exactly mimic the arguments of appendix A of Part I with virtually no change to show that, if there is spontaneous stochasticity, so that non-factorization occurs in (3.21) for a set of x of positive measure, then there exists a smooth function $\Theta = (\theta_0, \psi)$ on $\mathcal{S}$ which makes the variance (3.20) positive. This provides a positive lower bound to the global cumulative dissipation with that choice of Θ for a suitable subsequence $\nu_j, \kappa_j \to 0$.

Unfortunately, it seems to be very difficult to show that, with boundary conditions ψ fixed, spontaneous stochasticity implies anomalous dissipation for a suitable choice of initial data θ_0. The difficulties are made apparent by the following easily proved identity for the variance (3.20), which separates contributions from θ_0 and ψ:

$$
\begin{aligned}
\mathrm{Var}[\Theta(\tilde{\sigma}(x, t))] = {} & \mathrm{Var}[\theta_0(\tilde{\xi}_{t,0}(x)) | \tilde{\tau}(x, t) = 0] P(\tilde{\tau}(x, t) = 0) \\
& + \mathrm{Var}[\psi(\tilde{\xi}_{t, \tilde{\tau}(x,t)}(x), \tilde{\tau}(x, t)) | \tilde{\tau}(x, t) > 0] P(\tilde{\tau}(x, t) > 0).
\end{aligned}
$$
(C 1)

Here the variances are conditioned upon the events $\tilde{\tau}(x, t) = 0$ or $\tilde{\tau}(x, t) > 0$ and the symbol $P(\cdots)$ denotes the probability measure of these same events. By non-negativity of the variance, one readily obtains

$$
\mathrm{Var}[\Theta(\tilde{\sigma}(x, t))] \geqslant \mathrm{Var}[\theta_0(\tilde{\xi}_{t,0}(x)) | \tilde{\tau}(x, t) = 0] P(\tilde{\tau}(x, t) = 0).
$$
(C 2)

If one assumes that there is spontaneous stochasticity for the sub-ensembles specified by $\tilde{\tau}(\boldsymbol{x}, t) = 0$ for a positive-measure set of $\boldsymbol{x} \in \Omega$ (which is not an entirely straightforward assumption), then we can again use the arguments of Part I, appendix A to prove that

$$\lim_{j \to \infty} \text{Var}[\theta_0(\tilde{\boldsymbol{\xi}}_{t,0}^{\nu_j,\kappa_j}(\boldsymbol{x})) | \tilde{\tau}^{\nu_j,\kappa_j}(\boldsymbol{x}, t) = 0] > 0 \qquad (\text{C}\,3)$$

for a suitable smooth initial datum θ_0 and for a suitable subsequence $\nu_j, \kappa_j \to 0$, on a positive-measure set of $\boldsymbol{x} \in \Omega$. However, two difficulties appear. One is that, possibly,

$$\lim_{j \to \infty} P(\tilde{\tau}^{\nu_j,\kappa_j}(\boldsymbol{x}, t) = 0) = 0 \quad a.e.\ \boldsymbol{x} \in \Omega! \qquad (\text{C}\,4)$$

Another technical difficulty is that vague topology of Young measures can be used to establish convergence of the space average

$$\lim_{j \to \infty} \langle \text{Var}[\theta_0(\tilde{\boldsymbol{\xi}}_{t,0}^{\nu_j,\kappa_j}) | \tilde{\tau}^{\nu_j,\kappa_j}(t) = 0] \rangle_\Omega \qquad (\text{C}\,5)$$

whenever θ_0 is a continuous function, but to obtain convergence of the needed space average

$$\lim_{j \to \infty} \langle \text{Var}[\theta_0(\tilde{\boldsymbol{\xi}}_{t,0}^{\nu_j,\kappa_j}) | \tilde{\tau}^{\nu_j,\kappa_j}(t) = 0] P(\tilde{\tau}^{\nu_j,\kappa_j}(t) = 0) \rangle_\Omega \qquad (\text{C}\,6)$$

by using the same arguments, one must know that the functions

$$g^{\nu,\kappa}(\boldsymbol{x}, t) \equiv P(\tilde{\tau}^{\nu,\kappa}(\boldsymbol{x}, t) = 0) \qquad (\text{C}\,7)$$

converge as $\nu, \kappa \to 0$ to a continuous (non-zero) function $g(\boldsymbol{x}, t)$ uniformly in $\boldsymbol{x}$. This is a non-trivial statement which cannot be obtained by mere compactness arguments.

C.2. *Non-vanishing scalar sources*

To deal with scalar sources, we must introduce a new type of transition probability

$$q^{\nu,\kappa}(\tau, \boldsymbol{y}, s | \boldsymbol{x}, t) = \mathbb{E}[\delta(\tau - \tilde{\tau}(\boldsymbol{x}, t)) \delta^d(\boldsymbol{y} - \tilde{\boldsymbol{\xi}}_{t,s}(\boldsymbol{x}))], \quad \boldsymbol{y} \in \Omega, \ 0 \leqslant \tau < s < t, \qquad (\text{C}\,8)$$

which gives the joint probability for the particle released at $\boldsymbol{x}$ at time t to first hit the space boundary $\partial \Omega$ at time τ (going backward) and also to pass through point $\boldsymbol{y}$ at time s satisfying $\tau < s < t$. We can then rewrite the stochastic representation (3.5) as

$$\theta(\boldsymbol{x}, t) = \int_S H^d(\text{d}\boldsymbol{\sigma})\ \Theta(\boldsymbol{\sigma})\ q(\boldsymbol{\sigma} | \boldsymbol{x}, t) + \int_0^t \text{d}\tau \int_\tau^t \text{d}s \int_\Omega \text{d}^d y\ S(\boldsymbol{y}, s) q(\tau, \boldsymbol{y}, s | \boldsymbol{x}, t). \quad (\text{C}\,9)$$

To obtain a similar expression for the source variance term, we must introduce corresponding 2-time transition densities

$$\begin{aligned}
q_2^{\nu,\kappa}&(\tau; \boldsymbol{y}, s; \tau', \boldsymbol{y}', s' | \boldsymbol{x}, t) \\
&= \mathbb{E}[\delta(\tau - \tilde{\tau}(\boldsymbol{x}, t)) \delta^d(\boldsymbol{y} - \tilde{\boldsymbol{\xi}}_{t,s}(\boldsymbol{x})) \delta(\tau' - \tilde{\tau}(\boldsymbol{x}, t)) \delta^d(\boldsymbol{y}' - \tilde{\boldsymbol{\xi}}_{t,s'}(\boldsymbol{x}))], \\
&\quad \boldsymbol{y}, \boldsymbol{y}' \in \Omega, \ \tau < s < t, \tau' < s' < t, \qquad (\text{C}\,10)
\end{aligned}$$

and

$$q_2(\tau, \boldsymbol{y}, s; \tau', \boldsymbol{y}', s' | \boldsymbol{x}, t) = \delta(\tau - \tau') q_2(\tau; \boldsymbol{y}, s; \boldsymbol{y}', s' | \boldsymbol{x}, t). \qquad (\text{C}\,11)$$

With this quantity we can write

$$
\begin{aligned}
\mathrm{Var} & \left[\int_{\tilde{\tau}(\boldsymbol{x},t)}^{t} \mathrm{d}s \; S(\tilde{\boldsymbol{\xi}}_{t,s}(\boldsymbol{x}), s) \right] \\
& = \int_{0}^{t} \mathrm{d}\tau \int_{0}^{t} \mathrm{d}\tau' \int \mathrm{d}^{d}y \int \mathrm{d}^{d}y' \int_{\tau}^{t} \mathrm{d}s \int_{\tau'}^{t} \mathrm{d}s' \; S(\boldsymbol{y}, s) S(\boldsymbol{y}', s') \\
& \quad \times [q_2(\tau, \boldsymbol{y}, s; \tau', \boldsymbol{y}', s' | \boldsymbol{x}, t) - q(\tau, \boldsymbol{y}, s | \boldsymbol{x}, t) q(\tau', \boldsymbol{y}', s' | \boldsymbol{x}, t)].
\end{aligned}
\tag{C 12}
$$

We can also write the initial condition source covariance in a similar fashion, using the 2-time probability density

$$
q_2^{\nu,\kappa}(\boldsymbol{\sigma}; \tau', \boldsymbol{y}', s' | \boldsymbol{x}, t) = \mathbb{E}[\delta_{\mathcal{S}}(\boldsymbol{\sigma}, \tilde{\boldsymbol{\sigma}}(\boldsymbol{x}, t)) \, \delta(\tau' - \tilde{\tau}(\boldsymbol{x}', t)) \delta^{d}(\boldsymbol{y}' - \tilde{\boldsymbol{\xi}}_{t,s'}(\boldsymbol{x}'))],
\tag{C 13}
$$

which is proportional to $\delta(\tau - \tau')$, if we write $\boldsymbol{\sigma} = (\boldsymbol{y}, \tau)$. We have

$$
\begin{aligned}
\mathrm{Cov} & [\Theta(\tilde{\boldsymbol{\xi}}_{t,\tilde{\tau}(\boldsymbol{x},t)}(\boldsymbol{x}), \tilde{\tau}(\boldsymbol{x}, t)), \int_{\tilde{\tau}(\boldsymbol{x},t)}^{t} \mathrm{d}t' S(\tilde{\boldsymbol{\xi}}_{t,t'}(\boldsymbol{x}), t')] \\
& = \int_{\mathcal{S}} H^{d}(\mathrm{d}\boldsymbol{\sigma}) \int_{0}^{t} \mathrm{d}\tau' \int \mathrm{d}^{d}y' \int_{\tau'}^{t} \mathrm{d}s' \; \Theta(\boldsymbol{y}, s) S(\boldsymbol{y}', s') \\
& \quad \times [q_2(\boldsymbol{\sigma}; \tau', \boldsymbol{y}', s' | \boldsymbol{x}, t) - q(\boldsymbol{\sigma} | \boldsymbol{x}, t) q(\tau', \boldsymbol{y}', s' | \boldsymbol{x}, t)],
\end{aligned}
\tag{C 14}
$$

as the corresponding representation. The very close similarity of these formulae to those derived previously for advected scalars in flows without boundaries and for scalars with insulating/adiabatic walls allows us to prove that spontaneous stochasticity is sufficient for anomalous dissipation of passive scalars also for Dirichlet boundary conditions in the presence of smooth sources. The existence of a smooth source S on $\Omega \times [0, t]$ which makes the variance (C 12) positive is likewise shown by arguments like those in appendix A of Part I. We leave details to the reader. The statement here is that a smooth source S can be chosen for which there is anomalous scalar dissipation, either with zero initial boundary data or else with a smooth non-zero choice $\Theta = (\theta_0, \psi)$ of such data.

Appendix D. Numerical methods

D.1. *Methods for* §2.1

As in our previous numerical study of isotropic turbulence, we solve the stochastic equations (2.2) and (2.3) with interpolated velocities retrieved using the getVelocity database function. To solve these backward Itō stochastic differential equations (SDEs), we use a reflected time $\hat{s} = t_f - s$ which transforms them into forward Itō SDEs. To implement the reflecting boundary conditions at the channel walls we have found it convenient to use the very simple Euler algorithm of Lépingle (1995), which is ideally suited to the parallel plane boundaries of the channel flow. This method reduces to the standard Euler–Maruyma scheme at some specified small distance ϵ away from the walls. This algorithm (dropping hats on the reflected time) takes at the kth time step

$$
\tilde{\boldsymbol{\xi}}(s_{k+1}) = \tilde{\boldsymbol{\xi}}(s_k) + \Delta\tilde{\boldsymbol{\xi}}(s_{k+1}; s_k) + \kappa \boldsymbol{n}^{+} \, \Delta\tilde{\ell}^{+}(s_k) + \kappa \boldsymbol{n}^{-} \, \Delta\tilde{\ell}^{-}(s_k),
\tag{D 1}
$$

where $\Delta\tilde{\boldsymbol{\xi}}(s; s_k)$ is given by the Euler–Maruyama discretization

$$
\Delta\tilde{\boldsymbol{\xi}}(s; s_k) = \boldsymbol{u}(\tilde{\boldsymbol{\xi}}(s_k), s_k)(s - s_k) + \sqrt{2\kappa}(\widetilde{\boldsymbol{W}}(s) - \widetilde{\boldsymbol{W}}(s_k))
\tag{D 2}
$$

and where $\Delta\tilde{\ell}^{\pm}(s_k) = \tilde{\ell}^{\pm}(s_{k+1}) - \tilde{\ell}^{\pm}(s_k)$ is given by the Skorohod equation (see Karatzas & Shreve (1991, Lemma 3.6.14) and (A 26)):

$$\kappa\Delta\tilde{\ell}^{\pm}(s_k) = \max\left\{0, \max_{s_k \leqslant s \leqslant s_{k+1}}\left\{-\boldsymbol{n}^{\pm}\cdot[\tilde{\boldsymbol{\xi}}(s_k) + \Delta\tilde{\boldsymbol{\xi}}(s; s_k)]\right\} - h\right\}. \qquad (D\,3)$$

At the top wall $y = +h$, $\boldsymbol{n}^+ = -\hat{\boldsymbol{y}}$ and at the bottom wall $y = -h$, $\boldsymbol{n}^- = +\hat{\boldsymbol{y}}$. The stochastic solution of the Skorohod equation (D 3) is exactly realized by a closed formula involving an independent exponential random variable. See Lépingle (1995), Theorem 1. To minimize the additional computational cost of solving the Skorohod equation (D 3), the algorithm of Lépingle (1995) adds the local-time density terms into (D 1) only when the particle is within a distance ϵ of the walls, fixed independent of $\Delta s = s_{k+1} - s_k$ (In principle, the boundary local-time densities for channel flow that appear in figures 1 and 3 are thus a sum of contributions from both top and bottom walls. However, in practice, no particles released at the bottom wall were ever observed to be incident upon the top wall within the entire time available in the database and thus $\tilde{\ell}(s) = \tilde{\ell}^-(s)$. This is to be expected, since wall-normal velocities in turbulent channel flow generally have maximum magnitudes of order u_τ and, in the archived flow, advection at this maximum speed would require approximately double the archived time interval for a particle to transit from the bottom wall to the top wall.). We chose $\epsilon = 10\delta_\nu$ in our channel-flow simulations.

The Lépingle (1995) algorithm outlined above yields strong approximations to the joint process $(\tilde{\boldsymbol{\xi}}_{t,s}(\boldsymbol{x}), \tilde{\ell}_{t,s}(\boldsymbol{x}))$ for any $\boldsymbol{x}$. To study numerically the strong convergence of the approximate solutions of equations (D 1) and (D 3) for the results presented in figure 1, we first generated a realization of a Brownian motion $\widetilde{W}(s_i)$ sampled on an extremely fine grid of times s_i with a very small time step δs. We then applied the above algorithm of Lépingle (1995) for a larger time step $\Delta s = m\delta s$ which is a multiple of δs by a big integer m, using the same previously sampled Brownian motion $\widetilde{W}(s_i)$ for all $\Delta s = m\delta s$. We reduced the size of m until the numerical results for the joint process $(\tilde{\boldsymbol{\xi}}(s), \tilde{\ell}(s))$ were converged to within 0.1 %, which required a very small time step $\Delta s = 6.5 \times 10^{-6}$, or 1/1000th of the time between the stored database frames. The requirements are much less stringent for weak convergence of statistical averages over Brownian motions than for the strong convergence at fixed $\widetilde{W}_s$. The averages presented in §2.1 were calculated with a time step of $\Delta s = 2.1\bar{6} \times 10^{-3}$, or 1/3 of the time between database frames. To check for weak convergence, we numerically integrated the equations with double this time-step and found a relative change in the ensemble averages of less than 0.1 %.

The N-sample averages used for particle dispersions and PDFs were the same as those for isotropic turbulence discussed in appendix C of Part I. In particular, local-time PDFs were estimated with kernel density techniques. One key difference is that the absolute local times $|\tilde{\ell}_{t,0}|$ are positive quantities, so that their PDFs have a support boundary at 0 and naive application of kernel density estimators leads to 'seepage' of mass to negative values. Since the exact PDF is expected to have a maximum at 0 (highest probability for particles never to hit the wall), we employ the 'reflection method' (Karunamuni & Alberts 2005). This procedure involves performing the kernel density estimation on a symmetric dataset constructed by augmenting the original data by its negation. The optimal bandwidth was again chosen by the 'principle of minimal sensitivity'. Using these procedures and the same number of samples ($N = 1024$) as for channel flow, we were able to recover the analytical results in appendix A.3 for the PDF of local times of a Brownian motion on the half-axis reflected at the origin.
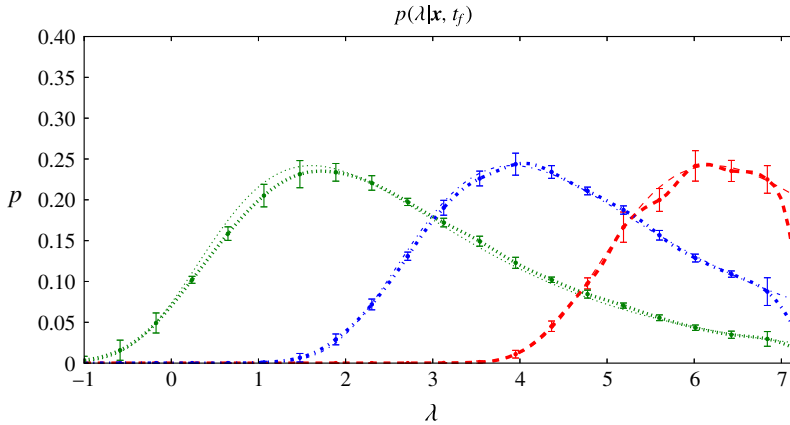
FIGURE 8. (Colour online) Hitting-time PDFs of Brownian motion for $Pr = 0.1$ (green, dot, $\cdots\cdots$), 1.0 (blue, dash-dot, — · —) and 10 (red, dash, - - - -). Numerical results are plotted with heavy lines, analytical results with light lines.

D.2. *Methods for* §*3.1*

To obtain the hitting times for channel flow from the numerical solution of the SDE (2.2) with the Euler–Maruyama scheme, we simply monitored the solution until the first time step where the y-component satisfied $\tilde{\eta}(s_k) > -h$ but $\tilde{\eta}(s_{k+1}) < -h$. We then stopped the integration and set $\tilde{\tau} = (s_k + s_{k+1})/2$. With a time step of $\Delta s = 2.1\bar{6} \times 10^{-3}$, this gives the hitting time accurately to within $1.08\bar{3} \times 10^{-3}$, or 5.41% of the viscous time τ_v. To obtain PDFs of $\lambda = \ln((t_f - \tau)/\tau_v)$ from the channel-flow data, we applied the same kernel density techniques as in appendix C of Part I. Note for Brownian motion (see (D 4) below) the mean hitting is infinite and with fluid advection the hitting times are expected to be even larger. Thus, many solutions do not ever hit the wall over the total time available in the channel-flow database and this necessitates a very large number of samples. The results presented in the text were for $N = 14\,336$ samples. The PDFs were verified to be converged with $\Delta s = 2.1\bar{6} \times 10^{-3}$ to within 0.1% and the plotted error bars represent both s.e.m. and the change due to 10% increase in h_*, as described in appendix D.1.

We applied identical numerical procedures to calculate the PDFs of $\lambda = \ln((t_f - \tau)/\tau_v)$ for a Brownian motion with diffusivity κ started at position $y > -h$ at time $t = t_f$ and going backward in time to $t = 0$. The analytical result to be used for comparison with channel flow is given by formula (3.23) with $x \to \Delta y := y + h > 0$, $t - s \to t_f - \tau$:

$$p^\kappa(\tau \mid y, t_f) = \begin{cases} \dfrac{\Delta y}{\sqrt{4\pi\kappa(t_f - \tau)^3}} \exp\left(-\dfrac{(\Delta y)^2}{4\kappa(t_f - \tau)}\right) & \tau < t_f \\ 0 & \tau > t_f \end{cases}. \qquad (D\,4)$$

Numerical and analytical results for Brownian motion are plotted together in figure 8. For $\lambda < 1.6$ one can see that the error from time discretization leads to a $\sim 5\%$ shift of the PDF to the right, toward larger hitting times. To correct this would require either a smaller time step or a more sophisticated stochastic interpolation scheme. For $\lambda > 6.5$, the lack of samples for $\lambda = \ln(t_f/\tau_v) \doteq 7.17$ leads the kernel density estimators to clearly underpredict the PDFs. Similar errors must exist in the channel-flow results.

REFERENCES

BERNARD, D., GAWĘDZKI, K. & KUPIAINEN, A. 1998 Slow modes in passive advection. *J. Stat. Phys.* **90**, 519–569.

BUARIA, D., YEUNG, P. K. & SAWFORD, B. L. 2016 A Lagrangian study of turbulent mixing: forward and backward dispersion of molecular trajectories in isotropic turbulence. *J. Fluid Mech.* **799**, 352–382.

BURDZY, K. 2009 Differentiability of stochastic flow of reflected Brownian motions. *Electron. J. Probab.* **14**, 2182–2240.

BURDZY, K., CHEN, Z.-Q. & SYLVESTER, J. 2004 The heat equation and reflected Brownian motion in time-dependent domains. *Ann. Prob.* **32** (1B), 775–804.

CADOT, O., COUDER, Y., DAERR, A., DOUADY, S. & TSINOBER, A. 1997 Energy injection in closed turbulent flows: stirring through boundary layers versus inertial stirring. *Phys. Rev.* E **56** (1), 427–433.

CONSTANTIN, P. & IYER, G. 2011 A stochastic-Lagrangian approach to the Navier–Stokes equations in domains with boundary. *Ann. Appl. Probab.* **21**, 1466–1492.

CORRSIN, S. 1953 Remarks on turbulent heat transfer. In *Proceeding of the Thermodynamics Symposium*, pp. 5–30. University of Iowa.

DRIVAS, T. D. & EYINK, G. L. 2017 A Lagrangian fluctuation–dissipation relation for scalar turbulence, I. Flows with no bounding walls. *J. Fluid Mech.* (submitted) arXiv:1606.00729.

ERDÉLYI, A. 1954 *Tables of Integral Transforms: Based, in Part, on Notes Left by Harry Bateman, California Institute of Technology. Bateman Manuscript Project* (ed. A. Erdélyi), W. Magnus, F. Oberhettinger, F. G. Tricomi, research associates, vol. 1. McGraw-Hill.

EYINK, G. L. 2008 Turbulent flow in pipes and channels as cross-stream 'inverse cascades' of vorticity. *Phys. Fluids* **20** (12), 125101.

EYINK, G. L. & DRIVAS, T. D. 2017 A Lagrangian fluctuation–dissipation relation for scalar turbulence, III. Turbulent Rayleigh–Bénard convection. *J. Fluid Mech.* (submitted) arXiv:1703.09604.

FREĬDLIN, M. I. 1985 *Functional Integration and Partial Differential Equations*. Princeton University Press.

FRIEDMAN, A. 2006 *Stochastic Differential Equations and Applications*. Dover.

GRAHAM, J., KANOV, K., YANG, X. I. A., LEE, M., MALAYA, N., LALESCU, C. C., BURNS, R., EYINK, G., SZALAY, A. & MOSER, R. D. 2016 A Web services accessible database of turbulent channel flow and its use for testing a new integral wall model for LES. *J. Turbul.* **17** (2), 181–215.

HSU, P. 1986 Brownian exit distribution of a ball. In *Seminar on Stochastic Processes, 1985*, pp. 108–116. Springer.

HUGGINS, E. R. 1970 Energy-dissipation theorem and detailed Josephson equation for ideal incompressible fluids. *Phys. Rev.* A **1** (2), 332.

KARATZAS, I. & SHREVE, S. E. 1991 *Brownian Motion and Stochastic Calculus*. Springer.

KARLIN, S. & TAYLOR, H. E. 1981 *A Second Course in Stochastic Processes*. Elsevier Science.

KARUNAMUNI, R. J & ALBERTS, T. 2005 On boundary correction in Kernel density estimation. *Stat. Meth.* **2** (3), 191–212.

KATZNELSON, Y. 2004 *An Introduction to Harmonic Analysis*. Cambridge University Press.

KEANINI, R. G. 2007 Random walk methods for scalar transport problems subject to Dirichlet, Neumann and mixed boundary conditions. *Proc. R. Soc. Lond.* A **463**, 435–460.

KLINE, S. J., REYNOLDS, W. C., SCHRAUB, F. A. & RUNDSTADLER, P. W. 1967 The structure of turbulent boundary layers. *J. Fluid Mech.* **30**, 74l–773.

KRAICHNAN, R. H. 1962 Turbulent thermal convection at arbitrary Prandtl number. *Phys. Fluids* **5** (11), 1374–1389.

KRAICHNAN, R. H. 1968 Small-scale structure of a scalar field convected by turbulence. *Phys. Fluids* **11**, 945–953.

KUNITA, H. 1997 *Stochastic Flows and Stochastic Differential Equations*, Cambridge Studies in Advanced Mathematics, vol. 24. Cambridge University Press.

Lépingle, D. 1995 Euler scheme for reflected stochastic differential equations. *Math. Comput. Simul.* **38** (1), 119–126.

Lions, P.-L. & Sznitman, A. S. 1984 Stochastic differential equations with reflecting boundary conditions. *Commun. Pure Appl. Maths* **37** (4), 511–537.

Mil'shtein, G. N. 1996 Application of the numerical integration of stochastic equations to solving boundary-value problems with Neumann's boundary conditions. *Teoriya Veroyatnostei i ee Primeneniya* **41** (1), 210–218.

Ng, E. W. & Geller, M. 1969 A table of integrals of the error functions. *J. Res. Natl Bur. Stand.* **73** (1), 1–20.

Niemela, J. J. & Sreenivasan, K. R. 2003 Confined turbulent convection. *J. Fluid Mech.* **481**, 355–384.

Oksendal, B. 2013 *Stochastic Differential Equations: An Introduction with Applications*. Springer Science & Business Media.

Pilipenko, A. 2014 *An Introduction to Stochastic Differential Equations with Reflection*. Potsdam University Press.

Pilipenko, A. Yu. 2005 Properties of the flows generated by stochastic equations with reflection. *Ukr. Math. J.* **57** (8), 1262–1274.

Richardson, L. F. 1926 Atmospheric diffusion shown on a distance-neighbor graph. *Proc. R. Soc. Lond.* A **110**, 709–737.

Rogers, L. C. G. & Williams, D. 2000 *Diffusions, Markov Processes and Martingales: Volume 2, Itô Calculus*. Cambridge University Press.

Schumacher, J. 2008 Lagrangian dispersion and heat transport in convective turbulence. *Phys. Rev. Lett.* **100** (13), 134502.

Schütz, S. & Bodenschatz, E. 2016 Two-particle dispersion in weakly turbulent thermal convection. *New J. Phys.* **18**, 065007.

Słomiński, L. 2013 Weak and strong approximations of reflected diffusions via penalization methods. *Stoch. Proc. Appl.* **123** (3), 752–763.

Soner, H. M. 2007 Stochastic representations for nonlinear parabolic PDEs. In *Handbook of Differential Equations: Evolutionary Equations*, vol. 3, pp. 477–526.

Spiegel, E. A. 1971 Convection in stars: I. Basic Boussinesq convection. *Annu. Rev. Astron. Astrophys.* **9** (1), 323–352.

Stroock, D. W. & Varadhan, S. S. 1971 Diffusion processes with boundary conditions. *Commun. Pure Appl. Maths* **24** (2), 147–225.

Taylor, G. I. 1932 The transport of vorticity and heat through fluids in turbulent motion. *Proc. R. Soc. Lond.* A **135** (828), 685–702.

Tsinober, A. 2009 *An Informal Conceptual Introduction to Turbulence*. Springer.